Time-dependent extension of Koopmans' picture for ionization by a laser pulse: Application to H2(B1Σu+)

Ingo Barth, Jörn Manz, Guennaddi Paramonov

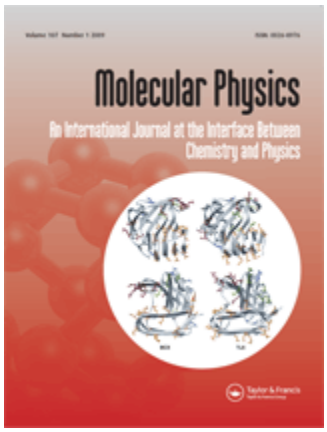

Time-dependent extension of Koopmans' picture for ionization by a laser pulse: Application to $H_2(B^1\Sigma_u^+)$

Journal:	*Molecular Physics*
Manuscript ID:	TMPH-2007-0315.R1
Manuscript Type:	Invited Article
Date Submitted by the Author:	05-Dec-2007
Complete List of Authors:	Barth, Ingo; Freie Universität Berlin, Institut für Chemie und Biochemie Manz, Jörn; Freie Universität Berlin, Institut für Chemie und Biochemie Paramonov, Guennaddi; National Academy of Sciences of Belarus, Institute of Physics; Freie Universität Berlin, Institut für Chemie und Biochemie
Keywords:	Single active electron, Ionization, Hydrogen molecule, Time-Dependent Extended Hartree-Fock, Koopmans' theorem
Note: The following files were submitted by the author for peer review, but cannot be converted to PDF. You must view these files (e.g. movies) online.	
SAE_H2_rev.tex SAE_H2.bib	

Time-dependent extension of Koopmans' picture for ionization by a laser pulse: Application to $H_2(B\,^1\Sigma_u^+)$

I. BARTH†, J. MANZ*† and G. K. PARAMONOV†‡

†Institut für Chemie und Biochemie, Freie Universität Berlin, Takustr. 3, 14195 Berlin, Germany
‡National Academy of Sciences of Belarus, Institute of Physics, Independence Ave. 70, 220602 Minsk, Republic of Belarus

Abstract

Koopmans' picture predicts that the i-th ionization potential IP_i is approximately equal to the negative orbital energy $-\epsilon_i$ of the molecular orbital φ_i occupied by the single active electron (SAE), which is ionized, $IP_i = -\epsilon_i$. The corresponding time-dependent extension describes ionization in terms of the time-dependent orbital $\varphi_i(t)$ which is occupied by the SAE starting from the Extended Hartree-Fock (EHF) wave-function. The Time-Dependent EHF-SAE theory for singlet states is developed, beyond previous TDHF-SAE approaches. Applications are demonstrated for ionization of (z-)aligned $H_2(B\,^1\Sigma_u^+)$, by means of linearly (z-)polarized laser pulses in the domain of dominant single photon ionization.

Keywords: Single active electron; Ionization; Hydrogen molecule; Time-Dependent Extended Hartree-Fock; Koopmans' theorem

1 Introduction

The purpose of this paper is to extend Koopmans' picture of ionization from the original time-independent presentation [1] to a new, time-dependent one. The traditional approach centered attention on the energetics. Accordingly, the i-th ionization potential IP_i is equal to the negative orbital energy $-\epsilon_i$ of the molecular orbital φ_i which is occupied initially by

*Corresponding author. Email: jmanz@chemie.fu-berlin.de

the single active electron (SAE) which is ionized, $IP_i = -\epsilon_i$. The success of Koopmans' picture rests on the approximate validity of several assumptions: (i) the initial molecular state is well described in terms of a single electronic configuration which is represented by a spin-adapted Slater determinant, (ii) ditto for the final ionic state, (iii) all other occupied molecular orbitals φ_k ($k \neq i$) are frozen, (iv) photoionization occurs as a Franck-Condon-type vertical transition, with frozen nuclei, (v) the frequency as well as (vi) the electric field strength, or the related intensity for photoionization are in the domain of single photon absorption. Specifically, Koopmans considered (vii) ionization by means of continuous wave excitation. It is well known that Koopmans' picture may break down if one or several of these conditions (i)–(vi) are not fulfilled [2].

Here we consider the same scenario (i)–(vi), except that (vii') ionization is induced by a laser pulse. This calls for a time-dependent extension of Koopmans' picture. The theory is developed in section 2, with applications to ionization of (z-)aligned H_2, starting from the electronic excited state $H_2(B\,^1\Sigma_u^+)$ in order to prepare the ion H_2^+ in the electronic ground state $H_2^+(X\,^2\Sigma_g^+)$. These initial and target states have been chosen because they are in accord with the necessary conditions (i)–(iii), and they allow rather easy choices of the laser parameters in order to fulfill also the remaining conditions (iv)–(vi). Specifically, we consider ionizations by ultrashort, five-cycle laser pulses with frequency corresponding to 8 eV photon energy, i.e. about 4 eV above the resonant zero electron kinetic energy (ZEKE) limit, and with sufficiently low field amplitudes, or corresponding low maximum intensities ($I_{max} < 10^{14}\,\mathrm{Wcm^{-2}}$) implying small ionization yields $Y \ll 1$, e.g. $Y = 0.1$.

For comparison, several quantum dynamics simulations of the ionization of H_2 have been published, starting from the electronic ground state $H_2(X^1\Sigma_g^+)$, see e.g. Refs. [3–15]. Again, conditions (i)–(iii) are fulfilled quite well, but the employed laser frequencies correspond to two or even multiphoton ionizations, which is in conflict with condition (v). To the best of our knowledge, single photon ionization of $H_2(X\,^1\Sigma_g^+)$ has been simulated so far only by two groups: Martín and coworkers [16, 17] employ rather high photon energies in the domains of $25 - 28$ eV or even $30 - 37$ eV, thus populating the $A\,^2\Sigma_u^+$ or Q_1 and Q_2 doubly excited autoionizing states, respectively, in very good agreement with the experimental results [17] but in conflict with condition (iii). In a recent seminal paper, Madsen and coworkers have applied the SAE limit of their Time-Dependent Hartree-Fock (TDHF) approach to single photon ionization of $H_2(X\,^1\Sigma_g^+)$ using 20 eV photon energy and $I_{max} = 10^{13}\,\mathrm{Wcm^{-2}}$ – this appears to be the first application of the TDHF-SAE approach which satifies all conditions (i)–(vi),(vii') [18], see also the discussion in section 2.

Our time-dependent extension of Koopmans' picture describes single electron ionization induced by a laser pulse in terms of the wavepacket dynamics of the single active electron (SAE) occupying the time-dependent orbital $\varphi_i(t)$, starting from the Extended Hartree-Fock (EHF) wavefunction and interacting with the nuclei as well as with all the other electron(s) which occupy the frozen orbital(s) φ_k. Our Time-Dependent EHF-SAE (TDEHF-SAE) approach describes laser induced transitions between singlet states, beyond previous TDHF-SAE theories [3, 18–21] which invoke artificial transitions e.g. from an initial singlet ground state to an excited singlet plus triplet superposition state, see the discussion below. The derivation is based on the Dirac-Frenkel variation principle applied

to the TDEHF-SAE wavefunction. The wavepacket $\varphi_i(t)$ is propagated on spatial and temporal grids using the method of Ref. [22], cf. section 2. This approach employs essentially the same concept as the original TDHF-SAE approach which has been suggested by Kulander [19–21], see also Refs. [3,18], but the "rigorous" TDEHF-SAE approach generates additional terms, e.g. the exchange term, in the equation of motion (EOM) of $\varphi_i(t)$ which are necessary to describe laser induced transitions between singlet states, beyond previous ones, see e.g. Refs. [3,18–21]; for extensions see also Ref. [12] and the literature cited therein. It is simpler than extensions to two or more time-dependent orbitals such as the (restricted) Time-Dependent Hartree-Fock (TDHF) [3,23] or (unrestricted) Time-Dependent Extended Hartree-Fock (TDEHF) approaches [11,24], the Time-Dependent Configuration Interaction (Singles) TD-CIS method [25,26], or the Time-Dependent analogue of the Complete Active Space Self Consistent Field (TD-CASSCF) method, also termed the Multi-Configuration Time-Dependent Hartree-Fock (MCTDHF) method [27–30]. It does not aim at describing double or multiple electron ionizations, cf. Ref. [11, 13]. Another SAE approach which employs equivalent concepts but uses entirely different techniques i.e. expansions in terms of molecular eigenstates states as well as dicretized continuum states has been developed by Saenz and coworkers, with good agreement with CI results [8]. Most importantly, our "rigorous" TDEHF-SAE approach takes into account explicitly all the related Coulomb and the exchange interactions of all electrons. Moreover, we do not invoke any other approximations such as reductions to 1D or 2D dimensionalities, or the use of screened Coulomb interactions, which have been made e.g. in Refs. [7,11,13].

The previous TDHF-SAE approaches [3,12,19–21] have been critized in the literature, see e.g. Refs. [30,31], but the apparent failures may well be due to inadequate applications to systems which are in conflict with the conditions (i)–(vi), or to one or the other of those additional approximations, cf. the successes reported by Saenz [8] and by Martín [14] and their coworkers. For comparison, accurate quantum simulations of the ionization of aligned $H_2(X\,^1\Sigma_g^+)$ by a laser pulse have already been carried out in full dimensionality i.e. 5D for the electrons [4–6, 8–10] or even 6D for the electrons plus nuclei [15, 16]. The numerical techniques of Refs. [4–6, 8–10, 15, 16] are designed, however, for quantum simulations of rather small systems, typically with two electrons; extended applications to larger systems with a dozen or more electrons would be very difficult if not even impossible, see e.g. the discussions in Refs. [10, 29]. The purpose of the present TDEHF-SAE method is of course not to compete against those descriptions of the ionizations of two electron systems. Instead, the present results should serve as a reference for rather straightforward extensions to ionization of multi-electron systems.

The model, theory, and techniques as well as the results, and the summary and outlook are presented in sections 2, 3 and 4, respectively.

2 Model, Theory, and Techniques

Before presenting the TDEHF-SAE extension of Koopmans' picture with application to ionization of $H_2(B\,^1\Sigma_u^+)$, it is important to demonstrate the approximate validity of the under-

lying conditions (i)–(vi), see section 1. For this purpose, we have carried out CASSCF(2,7) and Hartree-Fock (HF) calculations for H_2 and for H_2^+, respectively, using the aug-cc-pVQZ basis set and the Gaussian03 program package. The resulting bond distances and potential energies $R_{eX} = 1.4049\,a_0$ $(1.4011\,a_0)$, $V_X(R_{eX}) = -1.1700419\,E_h$ $(-1.1744746\,E_h)$ for $H_2(X\,^1\Sigma_g^+)$, $R_{eB} = 2.2998\,a_0$ $(2.43\,a_0)$, $V_B(R_{eB}) = -0.74785010\,E_h$ $(-0.7566611\,E_h)$ for $H_2(B\,^1\Sigma_u^+)$, and $R_{eX+} = 1.9977\,a_0$ $(1.9972\,a_0)$, $V_{X+}(R_{eX+}) = -0.60253560\,E_h$ $(-0.6026\,E_h)$ for $H_2^+(X\,^2\Sigma_g^+)$ agree well with accurate values (given in brackets) adapted from Refs. [32–34], respectively, see also the values which are tabulated in Ref. [35]. This confirms that the CASSCF and HF results may serve as adequate touch-stone for the criteria (i)–(iii). The corresponding resonance excitation energy at R_{eB} is $\hbar\omega_{res} = V_{X+}(R_{eB}) - V_B(R_{eB}) = 0.149002\,E_h = 4.05\,\mathrm{eV}$. For convenience, these results are illustrated in figure 1.

Condition (i) is fulfilled because the CASSCF wavefunction $\Psi_B(R_{eB})$ which represents the initial state $B\,^1\Sigma_u^+$ at R_{eB}, is well approximated by the spin-projected sum of Slater determinants (EHF wavefunction, see e.g. Ref. [36]) which are constructed by means of the corresponding orbitals $1\sigma_{gB}(R_{eB})$, $1\sigma_{uB}(R_{eB})$,

$$\begin{aligned}\Phi_B(R_{eB}) &= \frac{1}{\sqrt{2}}\big(|1\sigma_{gB}(R_{eB})\alpha, 1\sigma_{uB}(R_{eB})\beta| \\ &\qquad -|1\sigma_{gB}(R_{eB})\beta, 1\sigma_{uB}(R_{eB})\alpha|\big) \\ &= \frac{1}{\sqrt{2}}\big(|1\sigma_{gB}(R_{eB})\alpha, 1\sigma_{uB}(R_{eB})\beta| \\ &\qquad +|1\sigma_{uB}(R_{eB})\alpha, 1\sigma_{gB}(R_{eB})\beta|\big)\,. \end{aligned} \tag{1}$$

The corresponding overlap is $\langle\Psi_B(R_{eB})|\Phi_B(R_{eB})\rangle = 0.994$. (The Dirac brackets have their usual meaning, implying integration over all electronic degrees of freedom – here the spatial and spin variables $\mathbf{q}_i = (\mathbf{r}_i, \sigma_i)$ of two electrons $i = 1, 2$.) The subsequent derivations also profit from the adequate representation of the electronic ground state $\Psi_X(R_{eB})$ by a single Slater determinant (HF wavefunction), using the same orbitals $1\sigma_{gX}(R_{eB})$

$$\Phi_0 = \Phi_X(R_{eB}) = |1\sigma_{gX}(R_{eB})\alpha, 1\sigma_{gX}(R_{eB})\beta|, \tag{2}$$

with high overlap $\langle\Psi_X(R_{eB})|\Phi_X(R_{eB})\rangle = 0.951$.

Condition (ii) is fulfilled automatically because the ground state $X\,^2\Sigma_g^+$ of the cation H_2^+ at R_{eB} is represented by the proper one-electron wavefunction, denoted as $1\sigma_{gX+}(R_{eB})$. Finally, condition (iii) is also valid because the orbital $1\sigma_{gB}(R_{eB})$ which is occupied by the inactive electron of $H_2(B\,^1\Sigma_u^+)$ agrees well with $1\sigma_{gX+}(R_{eB})$. The corresponding overlap $\langle 1\sigma_{gB}(R_{eB})|1\sigma_{gX+}(R_{eB})\rangle = 0.9972$ shows that indeed, $1\sigma_{gB}(R_{eB})$ is a nearly perfectly frozen orbital. Likewise, it is also a very good approximation to $1\sigma_{gX}(R_{eB})$ representing the electronic ground state (2), $\langle 1\sigma_{gB}(R_{eB}))|1\sigma_{gX}(R_{eB})\rangle = 0.9832$, thus

$$\Psi_0 = |1\sigma_{gB}(R_{eB})\alpha, 1\sigma_{gB}(R_{eB})\beta| \approx \Phi_0. \tag{3}$$

For conditions (iv)–(vi), we consider ionization of the pre-excited and pre-z-aligned (cf. Ref. [37], [38]) molecule by a z-polarized five-cycle laser pulse, with z-component of the

electric field

$$E(t) \quad = \quad E_0 \sin(\omega t + \eta) \sin^2\left(\frac{t\pi}{t_p}\right) \tag{4}$$

where E_0 denotes the field amplitude corresponding to the upper limit of the intensity, to be referred to as maximum intensity,

$$I_{max} \quad = \quad \varepsilon_0 c E_0^2, \tag{5}$$

ω is the frequency, η the phase (set equal to zero), and $t_p = 5 \cdot 2\pi/\omega$ is the total pulse duration, corresponding to the mean duration $\tau = 0.364\, t_p$ and spectral width

$$\Gamma \quad \approx \quad \frac{9.051}{t_p}\hbar \approx \frac{3.295}{\tau}\hbar. \tag{6}$$

In order to satisfy conditions (v), we apply the frequency with photon energy $\hbar\omega = 8\,\mathrm{eV}$. For condition (vi), we use intensities below $3 \cdot 10^{13}$ Wcm^{-2} such that the ionization yields are much smaller than 1 (see section 3), i.e. we are in the domain of single photon ionization by ultrashort ($\tau = 0.94\,\mathrm{fs}$), broad ($\Gamma = 2.31\,\mathrm{eV}$) laser pulses. Accordingly, the target ion is prepared selectively in its electronic ground state, $H_2^+(X\,^2\Sigma_g^+)$; competing ionization channels such as ionic dissociation [7, 15, 16, 39] or double ionization with subsequent Coulomb explosion [4–7, 10, 11, 13, 40, 41] are negligible, see also Ref. [42].

Condition (iv) is also fulfilled because the vertical Franck-Condon (FC) transitions at R_{eB} (cf. equation (4)) prepare the cation with just a small stretch $R_{eB} - R_{eX+} = 0.3021\, a_0$ – this is close to the width $\sqrt{\hbar/(\mu\omega_B)} = 0.419\, a_0$ of the vibrational wavepacket of the $B\,^1\Sigma_u^+$ state – at the shallow attractive i.e. non-dissociative wall of the potential energy surface $V_{X+}(R)$. Here, the anharmonic vibrational period is $\tau_{X+} \approx 16\,\mathrm{fs}$, i.e. the nuclei appear to be nearly frozen during the pulse duration $\tau = 0.90\,\mathrm{fs}$. For comparison, FC-type ionization of the ubiquitous initial ground state $H_2(X\,^1\Sigma_g^+)$ would be less adequate because it would prepare the ion H_2^+ at the steep repulsive walls of the potential energy surfaces of the $X\,^2\Sigma_g^+$, or the more excited $A\,^2\Sigma_u^+$ or auto-ionizing Q_1 and Q_2 states, thus causing much faster nuclear motions or, ultimately, ultrafast ionic photodissociation [7, 15, 16, 39].

The present scenario, i.e. FC-type ionization

$$H_2(B^1\Sigma_u^+) \xrightarrow{\text{laser pulse}} H_2^+(X^2\Sigma_g^+) + e^- \tag{7}$$

at R_{eB} is illustrated in figure 1a, together with the spectrum of the laser pulse (4) which is evaluated as

$$E(\omega) \quad = \quad \left| \int_0^{t_p} E(t) e^{i\omega t} dt \right|^2. \tag{8}$$

Subsequently, the TDEHF-SAE theory of the time-dependent extension of Koopmans' picture is developed for the laser driven single active electron of H_2, using however the notations which allow further straightforward extensions to molecules with many electrons.

Accordingly, the laser driven, z-aligned H_2 molecule is described using fixed nuclear coordinates $\mathbf{R}_1 = -\mathbf{R}_2 = (0, 0, R_{eB}/2)$, and the coordinates $\mathbf{q}_i = (\mathbf{r}_i, \sigma_i)$ of electrons $i = 1, 2$. In spin-free approximation, the model Hamiltonian of the laser driven system is

$$H(t) = h^{(0)}(t) + \sum_{i=1}^{2} h^{(1)}(\mathbf{r}_i, t) + h^{(2)}(\mathbf{r}_1, \mathbf{r}_2). \quad (9)$$

The nuclear, zero-electron operator $h^{(0)}(t)$

$$h^{(0)}(t) = \frac{e^2}{4\pi\varepsilon_0}\frac{1}{|\mathbf{R}_1 - \mathbf{R}_2|} - \mathbf{E}(t)\mathbf{M}_n = h^{(0)} - \mathbf{E}(t)\mathbf{M}_n \quad (10)$$

describes, in general, the Coulomb repulsion of the nuclei, plus the interaction of the nuclear dipole $\mathbf{M}_n$ with the electric field $\mathbf{E}(t) = E(t)\mathbf{e}_z$. In the present case, $\mathbf{M}_n = 0$. The one-electron operators $h^{(1)}(\mathbf{r}_i, t)$ $(i = 1, 2)$

$$\begin{aligned} h^{(1)}(\mathbf{r}_i, t) &= T(\mathbf{r}_i) - \frac{e^2}{4\pi\varepsilon_0}\sum_{\alpha=1}^{2}\frac{1}{|\mathbf{r}_i - \mathbf{R}_\alpha|} + e\mathbf{E}(t)\mathbf{r}_i \\ &= h^{(1)}(\mathbf{r}_i) + e\mathbf{E}(t)\mathbf{r}_i \end{aligned} \quad (11)$$

account for the kinetic energy $T(\mathbf{r}_i) = -\hbar^2/(2m_e)\nabla_i^2$, the Coulomb attraction to the nuclei, and the interaction of the electric laser field with electron i, using the semiclassical dipole approaximation. Further extensions to laser vector potentials can be made e.g. as in Ref. [43]. The two-electron operators

$$h^{(2)}(\mathbf{r}_1, \mathbf{r}_2) = \frac{e^2}{4\pi\varepsilon_0}\frac{1}{|\mathbf{r}_i - \mathbf{r}_j|} = h^{(2)}(\mathbf{r}_2, \mathbf{r}_1) \quad (12)$$

describe the Coulomb repulsion of the electrons.

The time-dependent extension of Koopmans' picture assumes that the laser driven dynamics starts from the initial state (1) and evolves such that one electron occupies the frozen orbital $1\sigma_g = 1\sigma_{gB}(R_{eB})$, whereas the other one is the SAE which occupies the orbital $\tilde{\varphi}(t)$ starting from $\tilde{\varphi}(t = 0) = 1\sigma_u = 1\sigma_{uB}(R_{eB})$, thus

$$\Psi(t) = c_0(t)\Psi_0 + \frac{c_1(t)}{\sqrt{2}}(|\tilde{\varphi}(t)\alpha, 1\sigma_g\beta| + |1\sigma_g\alpha, \tilde{\varphi}(t)\beta|) \quad (13)$$

The TDEHF-SAE ansatz (13) takes into account that eventually, the laser might not only cause electronic excitations and ionizations which are expressed in terms of the SAE occupying $\tilde{\varphi}(t)$, but also stimulated emission back to the electronic ground state $X\,^1\Sigma_g^+$, cf. equation (3). The coefficients $c_0(t)$ and $c_1(t)$ yield the corresponding populations $P_i(t) = |c_i(t)|^2$ of the ground $(i = 0)$ and excited $(i = 1)$ states, with normalizations

$$P_0(t) + P_1(t) = 1, \quad (14)$$

and orthonormal orbitals

$$\begin{aligned} \langle 1\sigma_g|1\sigma_g\rangle &= 1, \\ \langle \tilde{\varphi}(t)|\tilde{\varphi}(t)\rangle &= 1, \\ \langle 1\sigma_g|\tilde{\varphi}(t)\rangle &= 0. \end{aligned} \tag{15}$$

Initially, $c_0(t=0)=0$ and $c_1(t=0)=1$.

Inserting the ansatz (13) into the time-dependet Schrödinger equation (TDSE)

$$i\hbar\frac{d}{dt}\Psi(t) = H(t)\Psi(t) \tag{16}$$

would yield, in principle, three coupled differential equations for the coefficients $c_0(t)$, $c_1(t)$, and for the orbital $\tilde{\varphi}(t)$ with constraints (14) and (15). The individual phases of $c_0(t)$, $c_1(t)$ and $\tilde{\varphi}(t)$ would be irrelevant, however; instead what really matters is the difference between the first and second components of $\Psi(t)$, equation (13), i.e. the phase of $c_0(t)$ minus the sum of the phases of $c_1(t)$ and $\tilde{\varphi}(t)$. In order to get rid of this redundance, and also for numerical convenience, we introduce the non-normalized orbital

$$\varphi(t) = \frac{c_0(t)}{2}1\sigma_g + \frac{c_1(t)}{\sqrt{2}}\tilde{\varphi}(t) \tag{17}$$

which incorporates all the relevant information about $c_0(t)$, $c_1(t)$, and $\tilde{\varphi}(t)$: Once $\varphi(t)$ is known, then first, $c_0(t)$ can be obtained by projecting $\varphi(t)$ on $1\sigma_g$; second, the absolute value of $c_1(t)$ can be obtained form the normalization (14); third, $\tilde{\varphi}(t)$ (including the irrelevant phase of $c_1(t)$) may be calculated from (17). Note that $\varphi(t)$ is not necessarily orthogonal to $1\sigma_g$. For simplicity, we shall say that the SAE occupies $\varphi(t)$ keeping in mind its decomposition (17). Inserting the Ansatz (17) into (13) yields the TDEHF-SAE wavefunction

$$\Psi(t) = |\varphi(t)\alpha, 1\sigma_g\beta| + |1\sigma_g\alpha, \varphi(t)\beta| \tag{18}$$

with the initial condition

$$\varphi(t=0) = \frac{1}{\sqrt{2}}1\sigma_u. \tag{19}$$

For comparison, the initial electronic ground state $X\,^1\Sigma_g^+$ could be represented by the alternative initial condition

$$\varphi(t=0) = \frac{1}{2}1\sigma_g. \tag{20}$$

The ansatz (18), or the equivalent one (13), is essential for our TDEHF-SAE-type extension of Koopmans' picture. Before deriving the corresponding equation of motion, it is illuminating to compare expression (18) with the TDHF-SAE ansatz [3, 18, 20]

$$\Psi_{TDHF}^{SAE}(t) = |\varphi(t)\alpha, 1\sigma_g\beta|\,. \tag{21}$$

It has two related physical problems which become evident for the ubiquitious scenario where the system is initially in the electronic ground state, i.e. $\varphi(t=0) = 1\sigma_g$ in equation (21) (compare with equation (20) for our alternative TDEHF-SAE approach). One of the electrons remains in the $1\sigma_g$ orbital, with specific spin, e.g. β. The other electron which occupies orbital $\varphi(t)$ is then partially or completely excited and ultimately ionized by the laser pulse. The ansatz (21) then implies the first problem i.e. the electron which has been ionized will be observed with specific spin, e.g. α. This is in conflict with experiments. Second, let us decompose $\varphi(t)$ into two parts i.e. the fraction which remains in the original orbital $1\sigma_g$ plus the other partial wave which describes excitation or ionization. Likewise, the Slater determinant (21) could be written as a sum of two contributions for the electronic ground and excited states. Obviously, both contributions have total spin z-components $M_S = 0$. Also, no doubt the ground state is a singlet state. It turns out, however, that the excited part of the Slater determinant (21) can be decomposed into two components describing singlet and triplet states, with equal weights. As a consequence, the TDHF-SAE ansatz (21) implies that all excitations or ionizations by the laser pulse are automatically associated with 50% spin-flip, from the initial singlet state to a triplet component. Again, this is in conflict with all experiments. In contrast, our TDEHF-SAE ansatz (13) or, equivalently, (18) avoids these problems, i.e. the ionized electron may be observed with equal probabilities for α or β spins, and the laser pulse drives the system exclusively from the initial to the final singlet states. The prize that we have to pay for the correct physical picture within our TDEHF-SAE approach is, however, a more elaborate equation of motion for the SAE occupying $\varphi(t)$.

In order to derive the TDEHF-SAE equation of motion of $\varphi(t)$, we use the Dirac-Frenkel variation principle. Varying (18) with respect to $\varphi(t)$ yields

$$\delta\Psi(t) \;=\; |\delta\varphi(t)\alpha, 1\sigma_g\beta| + |1\sigma_g\alpha, \delta\varphi(t)\beta| \,. \tag{22}$$

Projecting the TDSE (16) on (22) yields

$$i\hbar\langle\delta\Psi(t)|\dot{\Psi}(t)\rangle \;=\; \langle\delta\Psi(t)|H(t)|\Psi(t)\rangle \tag{23}$$

which may be rewritten as

$$i\hbar\langle\delta\varphi(t)|\dot{\varphi}(t)\rangle + i\hbar\langle 1\sigma_g|\dot{\varphi}(t)\rangle\langle\delta\varphi(t)|1\sigma_g\rangle \;=\; \frac{1}{2}\langle\delta\Psi(t)|H(t)|\Psi(t)\rangle. \tag{24}$$

Moreover, projecting the TDSE (16) on the electronic ground state (3) yields

$$i\hbar\langle\Psi_0|\dot{\Psi}(t)\rangle \;=\; \langle\Psi_0|H(t)|\Psi(t)\rangle \tag{25}$$

which may be rewritten as

$$i\hbar\langle 1\sigma_g|\dot{\varphi}(t)\rangle \;=\; \frac{1}{2}\langle\Psi_0|H(t)|\Psi(t)\rangle. \tag{26}$$

Inserting (26) into (24) yields

$$i\hbar\langle\delta\varphi(t)|\dot{\varphi}(t)\rangle \;=\; \frac{1}{2}\langle\delta\Psi(t)|H(t)|\Psi(t)\rangle - \frac{1}{2}\langle\Psi_0|H(t)|\Psi(t)\rangle\langle\delta\varphi(t)|1\sigma_g\rangle. \tag{27}$$

The matrix elements of the right hand side of equation (27) are evaluated, using the abbreviations

$$\begin{aligned} S_{\varphi_1(t)\varphi_2(t)} &= \langle\varphi_1(t)|\varphi_2(t)\rangle \\ &= \int \varphi_1^*(\mathbf{r},t)\varphi_2(\mathbf{r},t)d\mathbf{r}, \qquad (28) \\ h^{(1)}_{\varphi_1(t)\varphi_2(t)}(t) &= \langle\varphi_1(t)|h^{(1)}(t)|\varphi_2(t)\rangle \\ &= \int \varphi_1^*(\mathbf{r},t)h^{(1)}(\mathbf{r},t)\varphi_2(\mathbf{r},t)d\mathbf{r}, \qquad (29) \\ h^{(2)}_{\varphi_1(t)\varphi_2(t),\varphi_3(t)\varphi_4(t)} &= \langle\varphi_1(t)\varphi_3(t)|h^{(2)}|\varphi_2(t)\varphi_4(t)\rangle \\ &= \int\int \varphi_1^*(\mathbf{r}_1,t)\varphi_3^*(\mathbf{r}_2,t)h^{(2)}(\mathbf{r}_1,\mathbf{r}_2) \\ &\qquad \varphi_2(\mathbf{r}_1,t)\varphi_4(\mathbf{r}_2,t)d\mathbf{r}_1 d\mathbf{r}_2 \qquad (30) \end{aligned}$$

as

$$\begin{aligned} \frac{1}{2}\langle\Psi_0|H(t)|\Psi(t)\rangle &= S_{1\sigma_g\varphi(t)}h^{(0)} + S_{1\sigma_g\varphi(t)}h^{(1)}_{1\sigma_g 1\sigma_g}(t) \\ &\quad + h^{(1)}_{1\sigma_g\varphi(t)}(t) + h^{(2)}_{1\sigma_g 1\sigma_g,1\sigma_g\varphi(t)}, \qquad (31) \\ \frac{1}{2}\langle\delta\Psi(t)|H(t)|\Psi(t)\rangle &= S_{\delta\varphi(t)\varphi(t)}h^{(0)} + S_{1\sigma_g\varphi(t)}S_{\delta\varphi(t)1\sigma_g}h^{(0)} \\ &\quad + S_{\delta\varphi(t)\varphi(t)}h^{(1)}_{1\sigma_g 1\sigma_g}(t) + S_{\delta\varphi(t)1\sigma_g}h^{(1)}_{1\sigma_g\varphi(t)}(t) \\ &\quad + h^{(1)}_{\delta\varphi(t)\varphi(t)}(t) + S_{1\sigma_g\varphi(t)}h^{(1)}_{\delta\varphi(t)1\sigma_g}(t) \\ &\quad + h^{(2)}_{1\sigma_g 1\sigma_g,\delta\varphi(t)\varphi(t)} + h^{(2)}_{1\sigma_g\varphi(t),\delta\varphi(t)1\sigma_g}. \qquad (32) \end{aligned}$$

Inserting these matrix elements (31) and (32) into equation (27) and using $\langle 1\sigma_g|\mathbf{r}|1\sigma_g\rangle = 0$, thus $h^{(1)}_{1\sigma_g 1\sigma_g}(t) = h^{(1)}_{1\sigma_g 1\sigma_g}$, yields

$$\begin{aligned} i\hbar\langle\delta\varphi(t)|\dot{\varphi}(t)\rangle &= S_{\delta\varphi(t)\varphi(t)}h^{(0)} + S_{\delta\varphi(t)\varphi(t)}h^{(1)}_{1\sigma_g 1\sigma_g} + h^{(1)}_{\delta\varphi(t)\varphi(t)}(t) \\ &\quad + S_{1\sigma_g\varphi(t)}\left(h^{(1)}_{\delta\varphi(t)1\sigma_g}(t) - S_{\delta\varphi(t)1\sigma_g}h^{(1)}_{1\sigma_g 1\sigma_g}\right) \\ &\quad - S_{\delta\varphi(t)1\sigma_g}h^{(2)}_{1\sigma_g 1\sigma_g,1\sigma_g\varphi(t)} \\ &\quad + h^{(2)}_{1\sigma_g 1\sigma_g,\delta\varphi(t)\varphi(t)} + h^{(2)}_{1\sigma_g\varphi(t),\delta\varphi(t)1\sigma_g}. \qquad (33) \end{aligned}$$

Since $\delta\varphi(t)$ is arbitrary, it yields the final form of the TDEHF-SAE equation of motion for the orbital $\varphi(t) = \varphi(\mathbf{r},t)$

$$\begin{aligned} i\hbar\dot{\varphi}(t) &= \left(h^{(0)} + h^{(1)}_{1\sigma_g 1\sigma_g} + h^{(1)}(\mathbf{r},t)\right)\varphi(t) \\ &\quad + S_{1\sigma_g\varphi(t)}\left(h^{(1)}(\mathbf{r},t) - h^{(1)}_{1\sigma_g 1\sigma_g}\right)1\sigma_g \\ &\quad - h^{(2)}_{1\sigma_g 1\sigma_g,1\sigma_g\varphi(t)}1\sigma_g + J_{1\sigma_g}\varphi(t) + K_{1\sigma_g}\varphi(t) \qquad (34) \end{aligned}$$

where the Coulomb and exchange operators $J_{\varphi_1(t)}$ and $K_{\varphi_1(t)}$ are defined as

$$J_{\varphi_1(t)}\varphi_2(t) = \int h^{(2)}(\mathbf{r},\mathbf{r}')|\varphi_1(\mathbf{r}',t)|^2\varphi_2(\mathbf{r},t)d\mathbf{r}', \quad (35)$$

$$K_{\varphi_1(t)}\varphi_2(t) = \int h^{(2)}(\mathbf{r},\mathbf{r}')\varphi_1^*(\mathbf{r}',t)\varphi_2(\mathbf{r}',t)\varphi_1(\mathbf{r},t)d\mathbf{r}', \quad (36)$$

respectively. For fixed nuclei, the term $h^{(0)}+h^{(1)}_{1\sigma_g 1\sigma_g}$ in equation (34) is constant so that it can be taken into account as phase factor $\varphi(t)=\bar{\varphi}(t)\exp\left[-i\left(h^{(0)}+h^{(1)}_{1\sigma_g 1\sigma_g}\right)t/\hbar\right]$. The equation of motion for $\bar{\varphi}(t)$ is the same as for $\varphi(t)$, except for the elimination of the term $\left(h^{(0)}+h^{(1)}_{1\sigma_g 1\sigma_g}\right)\varphi(t)$ in equation (34).

Before proceeding to the results which can be derived from equation (34), let us compare the TDEHF-SAE equation of motion with the previous one derived from the TDHF-SAE approach [3, 18, 20]. The terms $h^{(1)}(\mathbf{r},t)\varphi(t)$ and $J_{1\sigma_g}\varphi(t)$ are common, but equation (34) has several additional terms, due to the ansatz (13), (18) compared to (21). The terms $S_{1\sigma_g\varphi(t)}$ and $h^{(2)}_{1\sigma_g 1\sigma_g,1\sigma_g\varphi(t)}$ turn out to be small in the present application, due to the near-orthogonality of $1\sigma_g$ and $\varphi(t)$ which describes ionization starting from $1\sigma_u$. The most important addition is the exchange term $K_{1\sigma_g}\varphi(t)$ which arises from the TDEHF-SAE ansatz (18). In contrast, the TDHF-SAE ansatz (21) does not yield this term, i.e. it is not adequate to describe even the present initial state (1).

For simplicity, we shall refer to equation (34) as "SAE equation", keeping in mind the decomposition (17) of $\varphi(t)$. Accordingly, the normalization of the wavefunction $\Psi(t)$ representing the frozen and active electrons, equations (13), (14), (17), is rewritten as

$$\langle\Psi(t)|\Psi(t)\rangle = 2S_{\varphi(t)\varphi(t)}+2|S_{1\sigma_g\varphi(t)}|^2=1. \quad (37)$$

As a test of its self-consistency, let us consider the time evolution of the model H_2 without any laser field, starting from the excited initial state $\Psi(t=0)=\Phi_B(R_{eB})$, cf. equations (1), (19). In this limit, the solution of the SAE equation (34) becomes

$$\varphi(t) = \frac{1}{\sqrt{2}}\,1\sigma_u\, e^{-iE_{H_2(B\,^1\Sigma_u^+)}t/\hbar} \quad (38)$$

and, therefore,

$$\Psi(t) = \Phi_B(R_{eB})e^{-iE_{H_2(B\,^1\Sigma_u^+)}t/\hbar} \quad (39)$$

where

$$\begin{aligned} E_{H_2(B\,^1\Sigma_u^+)} &= h^{(0)}+h^{(1)}_{1\sigma_g 1\sigma_g}+h^{(1)}_{1\sigma_u 1\sigma_u}+J_{1\sigma_g 1\sigma_u}+K_{1\sigma_g 1\sigma_u} \\ &= h^{(0)}+h^{(1)}_{1\sigma_g,1\sigma_g}+\epsilon_{1\sigma_u}, \quad (40) \\ J_{\varphi_1(t)\varphi_2(t)} &= \langle\varphi_2(t)|J_{\varphi_1(t)}|\varphi_2(t)\rangle = h^{(2)}_{\varphi_1(t)\varphi_1(t),\varphi_2(t)\varphi_2(t)}, \quad (41) \\ K_{\varphi_1(t)\varphi_2(t)} &= \langle\varphi_2(t)|K_{\varphi_1(t)}|\varphi_2(t)\rangle = h^{(2)}_{\varphi_1(t)\varphi_2(t),\varphi_2(t)\varphi_1(t)}, \quad (42) \end{aligned}$$

and $\epsilon_{1\sigma_u}$ is the orbital energy of the orbital $1\sigma_u$, i.e. $\Phi_B(R_{eB})$ is an eigenstate with the energy $E_{H_2(B\,^1\Sigma_u^+)}$ of the excited $H_2(B\,^1\Sigma_u^+)$, at the EHF level of theory.

Another test of self-consistency is provided by the other extreme case where a weak but sufficiently long laser pulse has achieved complete ionization. Subsequently, $\varphi(t) = \varphi_{as}(t)$ describes essentially a free-asymptotic wavepacket, far away from the ionic core H_2^+ ($|\mathbf{r} - \mathbf{R}_\alpha| \to \infty$) which is characterized by its asymptotic mean kinetic energy

$$T_{as} = \langle\varphi_{as}(t)|T|\varphi_{as}(t)\rangle. \tag{43}$$

In this limit, all terms $S_{1\sigma_g\varphi_{as}(t)}$, $h^{(2)}_{1\sigma_g 1\sigma_g, 1\sigma_g\varphi_{as}(t)}$, $J_{1\sigma_g}\varphi_{as}(t)$ and $K_{1\sigma_g}\varphi_{as}(t)$ in equation (34) vanish, i.e. $\varphi_{as}(t)$ is described by the asymptotic equation of motion

$$i\hbar\dot{\varphi}_{as}(t) = \left(h^{(0)} + h^{(1)}_{1\sigma_g 1\sigma_g} + T(\mathbf{r})\right)\varphi_{as}(t). \tag{44}$$

The corresponding total energy of the system (H_2^+ ion core plus asymptotic free electron) is

$$E_{as} = h^{(0)} + h^{(1)}_{1\sigma_g 1\sigma_g} + T_{as} = E_{H_2^+(X^2\Sigma_g^+)} + T_{as} = E_{ion} + T_{as} \tag{45}$$

and the corresponding ionization potential at R_{eB} is

$$\begin{aligned} IP_{B\,^1\Sigma_u^+} &= E_{as} - T_{as} - E_{H_2(B\,^1\Sigma_u^+)} \\ &= E_{H_2^+(X\,^2\Sigma_g^+)} - E_{H_2(B\,^1\Sigma_u^+)} = \left(h^{(0)} + h^{(1)}_{1\sigma_g 1\sigma_g}\right) - E_{H_2(B\,^1\Sigma_u^+)} \\ &= -\left(h^{(1)}_{1\sigma_u 1\sigma_u} + J_{1\sigma_g 1\sigma_u} + K_{1\sigma_g 1\sigma_u}\right) = -\epsilon_{1\sigma_u} \end{aligned} \tag{46}$$

in accord with Koopmans' theorem. The corresponding autocorrelation function is

$$C(t) = \langle\Psi(0)|\Psi(t)\rangle = e^{-iE_{H_2(B\,^1\Sigma_u^+)}t/\hbar}. \tag{47}$$

In general, a laser pulse will induce non-stationary dynamics. This has many consequences including electronic excitation and ionization. These processes are associated with corresponding changes of the mean energy

$$\begin{aligned} E(t) &= \langle\Psi(t)|H(t)|\Psi(t)\rangle \\ &= h^{(0)} + h^{(1)}_{1\sigma_g 1\sigma_g} - 2|S_{1\sigma_g\varphi(t)}|^2 h^{(1)}_{1\sigma_g 1\sigma_g} + 2h^{(1)}_{\varphi(t)\varphi(t)}(t) \\ &\quad +4\mathrm{Re}\left(S_{1\sigma_g\varphi(t)}h^{(1)}_{\varphi(t)1\sigma_g}(t)\right) + 2J_{1\sigma_g\varphi(t)} + 2K_{1\sigma_g\varphi(t)}, \end{aligned} \tag{48}$$

of the mean z-component of the dipole, $M_{nz} - M_{ez} = 0 - e(z_1 + z_2)$ (the other x- and y-components vanish for symmetry reasons)

$$\begin{aligned} M_z(t) &= \langle\Psi(t)| - e(z_1 + z_2)|\Psi(t)\rangle \\ &= -2e\langle\varphi(t)|z|\varphi(t)\rangle - 4e\,\mathrm{Re}\left(S_{1\sigma_g\varphi(t)}\langle\varphi(t)|z|1\sigma_g\rangle\right), \end{aligned} \tag{49}$$

and of the autocorrelation function

$$\begin{aligned} C(t) &= \langle\Psi(0)|\Psi(t)\rangle = 2\left(S_{\varphi(0)\varphi(t)} + S_{\varphi(0)1\sigma_g} S_{1\sigma_g\varphi(t)}\right) \\ &= 2S_{\varphi(0)\varphi(t)} = \sqrt{2} S_{1\sigma_u\varphi(t)}, \end{aligned} \tag{50}$$

starting from the initial values

$$E(0) = E_{H_2(B\,^1\Sigma_u^+)} \tag{51}$$

$$M_z(0) = 0, \tag{52}$$

and

$$C(0) = 1, \tag{53}$$

respectively. The mean energy (equation (48)) consists of the time-independent Coulomb repulsion of the nuclei (first term), the time-independent kinetic energy of the inactive electron in the frozen orbital $1\sigma_g$ with Coulomb attraction to the nuclei (second term), the kinetic energy of the active electron in the time-dependent orbital $\varphi(t)$ with Coulomb attraction to the nuclei and interaction with the electric field (third, forth, and fifth terms), and the Coulomb (sixth term) and exchange (seventh term) energies between inactive and active electrons. Note that for the electronic ground state, the exchange and the Coulomb energies are identical. The calculations of the dipole function (49) are carried out using the effective charge $-e(1+m_e/(m_e+2m_p))$, as suggested in Ref. [22], with marginal deviations from the electron charge $-e$.

Another possible consequence of electronic excitation and ionization is symmetry breaking. Accordingly, the laser pulse transforms the initial ungerade, bound eigenstate $\Psi(0) = \Phi_B(R_{eB})$ into a time-dependent wavefunction which can be written either as superposition of gerade plus ungerade components, or as bound plus ionized partial waves, or both,

$$\begin{aligned} \Psi(t) &= \Psi_g(t) + \Psi_u(t) \\ &= \Psi_{bound,g}(t) + \Psi_{ion,g}(t) + \Psi_{bound,u}(t) + \Psi_{ion,u}(t) \\ &= \Psi_{bound}(t) + \Psi_{ion}(t). \end{aligned} \tag{54}$$

Furthermore, the total wavefunction as well as its symmetry adapted bound and ionized partial waves can be expanded in terms of corresponding symmetry adapted bound and ionized eigenstates,

$$\Psi_{bound,s}(t) = \sum_j c_{s,j}(t)\, e^{-iE_{s,j}(t-t_p)/\hbar} \Phi_{s,j} \tag{55}$$

and

$$\Psi_{ion,s}(t) = \int_{E_{ion}}^{\infty} c_{s,E}(t)\, e^{-iE(t-t_p)/\hbar} \Phi_{s,E}\, dE \tag{56}$$

for symmetries $s = g$ and $s = u$, respectively. According to the TDEHF-SAE ansatz (18), the expansions (55) and (56) are restricted, however, to corresponding representations of the eigenstates $\Phi_{s,j}$ and $\Phi_{s,E}$ in terms of two Slater determinants describing singlet states and single excitations, with energies $E_{s,j}$ and E, respectively. Their expansion coefficients $c_{s,j}(t)$ and $c_{s,E}(t)$ are determined by the laser pulse during $0 \le t \le t_p$, without any further changes during subsequent field-free evolutions. For $t \ge t_p$, this allows the simplified notations $c_{s,j}(t) = c_{s,j}(t_p) = c_{s,j}$ and $c_{s,E}(t) = c_{s,E}(t_p) = c_{s,E}$. The lower integration limit in equation (56) is the ionization threshold $E_{ion} = h^{(0)} + h^{(1)}_{1\sigma_g 1\sigma_g} = -0.5988\, E_h$ at R_{eB}.

The TDEHF-SAE ansatz (18) also suggests an alternative way of writing the gerade and ungerade components of $\Psi(t)$, in terms of corresponding gerade and ungerade components of the TDEHF-SAE wave function

$$\varphi(t) \;=\; \varphi_g(t) + \varphi_u(t), \tag{57}$$

thus

$$\Psi_s(t) \;=\; |\varphi_s(t)\alpha, 1\sigma_g\beta| + |1\sigma_g\alpha, \varphi_s(t)\beta| \tag{58}$$

for $s = g$ and $s = u$. The symmetry adapted components of $\varphi(t)$ can be determined using symmetry projection operators

$$\varphi_g(t) \;=\; \hat{P}_g\varphi(t) = \frac{1}{2}(1 + I)\varphi(t) \tag{59}$$

and

$$\varphi_u(t) \;=\; \hat{P}_u\varphi(t) = \frac{1}{2}(1 - I)\varphi(t) \tag{60}$$

where I denotes inversion. The corresponding probabilities of observing components with $s = g$ or $s = u$ symmetries are

$$P_s(t) \;=\; 2S_{\varphi_s(t)\varphi_s(t)} + 2|S_{1\sigma_g\varphi_s(t)}|^2, \tag{61}$$

compare with equation (37). Accordingly, the normalization $P_g(t) + P_u(t) = 1$ is satisfied automatically.

The SAE equation (34) is propagated using the method of Ref. [22], with equidistant temporal grid, $\Delta t = 0.01026\,\hbar/E_h$. For this purpose, the frozen and active electrons are described in terms of cylindrical coordinates z_i, ρ_i, ϕ_i $(i = 1, 2)$, using spatial grids, which should be large enough such that the laser driven wavepacket does not enter the narrow layers which are defined as so-called gobbler domains (see below) close to the grid boundaries during the laser pulse; for a quantitative definition, see equation (68) below. Specifically, we employ $N_z = 200$ and $N_\rho = 150$ grid points between the grid boundaries $z_{min} = -96.696\, a_0$ and $z_{max} = +96.696\, a_0$ as well as $\rho_{min} = 0.29404\, a_0$ and $\rho_{max} = 71.686\, a_0$ for the coordinates z and ρ, respectively. The value ρ_{min} is introduced in order to avoid any numerical problems due to the divergences of the Coulomb interactions for coinciding

particles, i.e. numerically, the electrons never coincide with the nuclei. Moreover, any possible coincidences of the two electrons on the same grid points are eliminated because that would never occur in reality. The results which are obtained for these parameters have been tested for convergence with respect to the time step Δt, and also the parameters for the grid boundaries, and the numbers of grid points per degree of freedom, respectively.

In order to avoid artificial back scattering of the wave function $\varphi(t)$ from the grid boundaries at z_{min}, z_{max} or ρ_{max}, we employ the method of Manolopoulos [44]. For this purpose, all grid points within narrow layers parallel to the grid boundaries are treated as "gobbler" domains. Specifically, we employ gobbler layers with seven grid points perpendicular to the grid boundaries, i.e. grid points $1-7$ as well as $194-200$ along z, and likewise grid points $144-150$ along ρ. The corresponding grid domains (denoted by subscript gr) for representing $\varphi(t)$ but excluding the gobbler domains are thus reduced to $z_{min,gr} = -85.227\,a_0 \le z \le z_{max,gr} = 85.227\,a_0$ and $\rho_{min,gr} = \rho_{min} \le \rho \le \rho_{max,gr} = 65.285\,a_0$. In addition to the corresponding widths of the gobbler domains, the other independent parameter of the method of Manolopoulos [44] is the minimum kinetic energy of the electrons at the grid boundaries. For the present application to ionization, this is equal to minus the maximum value of the (negative) Coulomb potential energy at the edge of the gobbler layers. To the best of our knowledge, this is the first application of that method to laser driven electrons. Gratifyingly, we could verify that indeed, suppression of back-scattering of the wavepackets from the grid boundaries turns out to be perfect.

Since the laser is polarized along the z-axis, it does not change the σ-type cylindrical symmetry of $\varphi(t)$, i.e. the frozen and active orbitals $1\sigma_g$ and $\varphi(t)$ keep their initial axial symmetry. This allows to reduce the three- and six-dimensional integrals (28), (29), (35), (36) and (30), (41), (42) to two- and five-dimensional ones, using the analytical results $\int_0^{2\pi} d\phi = 2\pi$ and $\int_0^{2\pi} d\phi' = 2\pi$, $\phi' = (\phi_1 + \phi_2)/2$, respectively. The integral of the complementary angular variable $\phi'' = (\phi_1 - \phi_2)/2$, $-\pi \le \phi'' \le \pi$ is carried out using an equidistant grid representation with $N_{\phi''} = 500$ grid points. These reduced two- and five-dimensional integrals are evaluated using the routine DGQRUL of the IMSL library for the grid that is used to represent $\varphi(t)$, i.e. excluding the gobbler domains. The corresponding numerical results are denoted with the subscript gr, for example,

$$S_{\varphi(t)\varphi(t),gr} \;=\; \langle\varphi(t)|\varphi(t)\rangle_{gr} = 2\pi \int_{z_{min,gr}}^{z_{max,gr}} \int_{\rho_{min,gr}}^{\rho_{max,gr}} |\varphi(t)|^2\, \rho\, d\rho\, dz, \qquad (62)$$

cf. equation (28). Integrals which involve the frozen orbital may be evaluated accurately within even smaller domains of the $1\sigma_g$ orbital; in practice we employ the boundaries $z_{min,1\sigma_g} = -8.2457\,a_0 \le z \le z_{max,1\sigma_g} = 8.2457\,a_0$ and $\rho_{min} \le \rho \le \rho_{max,1\sigma_g} = 8.7598\,a_0$.

After the laser pulse, some parts of the laser driven wavepacket $\varphi(t)$ which represents the active electron have gained sufficient energy $E > E_{ion}$ such that they will ionize. The corresponding fractions of the ionization yields which ionize perpendicular to the zone boundaries at $z_{min,gr}$, $z_{max,gr}$ and $\rho_{max,gr}$ till time t are denoted as $Y_{z(-)}(t)$, $Y_{z(+)}(t)$ and $Y_\rho(t)$, respectively. They are evaluated as time-integrated fluxes perpendicular to the zone boundaries, just before entering the respective gobbler domains, cf. Ref. [22]. The total

ionization yield till time t is evaluated as

$$Y_{total}(t) \quad = \quad Y_{z(-)}(t) + Y_{z(+)}(t) + Y_{\rho}(t). \tag{63}$$

Flux conservation requires that this total ionization yield is equal to the loss of the density of the wave function, integrated over the grid domain,

$$\begin{aligned} Y_{total,gr}(t) &= 1 - P_{gr}(t) \\ &= 1 - \langle \Psi(t) | \Psi(t) \rangle_{gr} \\ &= 1 - 2S_{\varphi(t)\varphi(t),gr} - 2|S_{1\sigma_g\varphi(t),gr}|^2, \end{aligned} \tag{64}$$

cf. equation (37). In the applications, excellent agreement of $Y_{total}(t)$ and $Y_{total,gr}(t)$ (equations (63), (64)) serves as numerical test of consistency. As a caveat we note, however, that both expressions (63) and (64) suffer from the numerical restrictions of the finite grid. This may lead to artifacts if the laser pulse populates bound Rydberg states which extend beyond the grid domains. These Rydberg states would be "eaten up" in the gobbler domains, as if they contribute to ionization. The numerical results based on expressions (63) and (64) would thus overestimate the true ion yields. In practice, we avoid this problem by chosing laser parameters $\hbar\omega$ and t_p such that the power spectrum of the laser pulse is well above the ionization threshold,

$$\hbar\omega - \Gamma/2 \quad > \quad IP_{B^1\Sigma_u^+}, \tag{65}$$

cf. equations (4)–(6), (46). Rigorously, the asymptotic value of the ionization yield Y_{total} should extrapolated from expressions (63) or (64) as

$$Y_{total} \quad = \quad \lim_{t\to\infty} Y_{total}(t). \tag{66}$$

In practice, the numerical value of the ionization yield does not rise before the time t_{gr} when the ionized electron arrives at the grid boundaries,

$$Y_{total}(t) \quad \approx \quad 0 \qquad \text{for} \qquad 0 \le t \le t_{gr}, \tag{67}$$

where the grid is chosen large enough such that

$$t_p \quad \le \quad t_{gr}. \tag{68}$$

Subsequently, the electrons which get ionized reach the grid boundary, and $Y_{total}(t)$ increases monotonically until it reaches the asymptotic plateau

$$Y_{total,as} \quad = \quad Y_{total}(t_{as}), \tag{69}$$

where t_{as} is sufficiently large. The present results were obtained using $t_{as} = 15.5\,\text{fs}$. Note that the $Y_{total,as}$ is a lower limit,

$$Y_{total,as} \quad < \quad Y_{total}, \tag{70}$$

because a small fraction of the electronic flux with small momenta may leave the grid even after t_{as}.

An alternative method for calculating Y_{total} is based on the decomposition of the total wave function $\Psi(t)$ after the end of the laser pulse ($t \geq t_p$) in terms of its bound and ionized components; for illuminating discussions of the associated symmetries, we shall present this derivation with an extended consideration of the corresponding gerade and ungerade partial waves, see equation (54). Accordingly, let us consider the autocorrelation functions of the wavefunction after the end of the laser pulse

$$\begin{aligned} C_{t_p}(t) &= \langle \Psi(t_p) | \Psi(t) \rangle = C_{t_p,g}(t) + C_{t_p,u}(t) \qquad (t \geq t_p) \\ &= 2 \left(S_{\varphi(t_p)\varphi(t)} + S_{\varphi(t_p)1\sigma_g} S_{1\sigma_g \varphi(t)} \right), \end{aligned} \tag{71}$$

again with gerade ($s = g$) and ungerade ($s = u$) components

$$\begin{aligned} C_{t_p,s}(t) &= \langle \Psi_s(t_p) | \Psi_s(t) \rangle \\ &= \sum_j |c_{s,j}|^2 e^{-iE_{s,j}(t-t_p)/\hbar} + \int_{E_{ion}}^{\infty} |c_{s,E}|^2 e^{-iE(t-t_p)/\hbar} \, dE \\ &= 2 \left(S_{\varphi(t_p)\varphi_s(t)} + S_{\varphi(t_p)1\sigma_g} S_{1\sigma_g \varphi_s(t)} \right). \end{aligned} \tag{72}$$

The second equation (72) is based on the orthogonality of the basis functions which are used in the expansions (55), (56). As a caveat which is equivalent to the previous one (see the discussion of equations (63), (64)), we note that the numerical restriction to a finite grid implies that the assumption of orthogonality is not satisfied for Rydberg wavefunctions which extend beyond the grid boundaries. The results derived from the expression (72) may suffer from this shortcoming. In practice, we avoid this problem by applications to laser pulse which do not populate any Rydberg states, cf. equation (65). The third equation (72) is analogous to equation (50) and allows the evaluation of the autocorrelation function in terms of the symmetry projected solutions of the SAE equation $\varphi_s(t)$, cf. equations (34), (59) and (60). Furthermore, we make use of the condition that the electron does not leave the grid domain before the end of the laser pulse $t_p \leq t_{gr}$, i.e. $\langle \Psi(t_p) | \Psi(t_p) \rangle_{gr} = 1$, cf. equations (64), (67), (68). In this case, the autocorrelation functions (71) and (72) can be rewritten as

$$C_{t_p}(t) = \langle \Psi(t_p) | \Psi(t) \rangle = \langle \Psi(t_p) | \Psi(t) \rangle_{gr}, \tag{73}$$

$$C_{t_p,s}(t) = \langle \Psi_s(t_p) | \Psi_s(t) \rangle = \langle \Psi_s(t_p) | \Psi_s(t) \rangle_{gr}. \tag{74}$$

Fourier transformation of the autocorrelation functions yields the corresponding "spectrum"

$$\alpha(\omega) = \alpha_g(\omega) + \alpha_u(\omega) \tag{75}$$

with symmetry adapted components

$$\begin{aligned} \alpha_s(\omega) &= \frac{1}{2\pi} \int_{t_p - T}^{t_p + T} e^{i\omega t} C_{t_p,s}(t) \, dt \\ &= \sum_j |c_{s,j}|^2 \delta(\omega - E_{s,j}/\hbar) + \int_{E_{ion}}^{\infty} |c_{s,E}|^2 \delta(\omega - E/\hbar) \, dE \end{aligned} \tag{76}$$

in the ideal case, $T \to \infty$. In practice, however, the SAE equation can be propagated only during a finite time T after the laser pulse, e.g. $T = 90\,\mathrm{fs}$ for the applications below. Accordingly, the δ distributions are replaced by spectral peaks with shapes $\sin\left[(\omega - E_{s,j}/\hbar)T\right] / \left[(\omega - E_{s,j}/\hbar)T\right]$, with finite values for the maxima and for the spectral widths

$$\Gamma_T = \frac{3.791}{T}\,\hbar, \tag{77}$$

e.g. $\Gamma_T = 0.028\,\mathrm{eV}$ for $T = 90\,\mathrm{fs}$. An important condition for adequate resolutions of the subsequent results is that the width Γ_T of the spectral method is smaller than the width Γ of the laser pulse, equation (6). In the subsequent applications, this condition is always fulfilled i.e. $\Gamma_T = 0.028\,\mathrm{eV} \ll 2.31\,\mathrm{eV} = \Gamma$. In principle, these symmetry adapted spectra (76) contain important information about the energy levels $E_{s,j}$ or E for bound and ionized electronic states with symmetry s, and the corresponding populations

$$P_{s,j} = |c_{s,j}|^2, \tag{78}$$

and

$$P_{s,E} = |c_{s,E}|^2 \tag{79}$$

after the end of the laser pulse ($t \geq t_p$), within the SAE approximation, equation (18), and provided that the laser pulse does not populate any Rydberg states which extend beyond the grid boundaries.

Integration of the spectra (76) over frequencies with photon energies below or above the ionization threshold yields the corresponding probabilities for electronic excitation versus ionization by the laser pulse, with corresponding gerade and ungerade components given by

$$P_{bound} = P_{bound,g} + P_{bound,u} \tag{80}$$

and

$$P_{ion} = P_{ion,g} + P_{ion,u} \tag{81}$$

where

$$P_{bound,s} = \sum_j P_{s,j} \tag{82}$$

and

$$P_{ion,s} = \int_{E_{ion}}^{\infty} P_{s,E}\, dE, \tag{83}$$

respectively, for $s = g$ and $s = u$, cf. equations (76)–(79). Likewise, the probabilites of observing symmetries $s = g$ or $s = u$ are

$$P_s = P_{bound,s} + P_{ion,s}, \tag{84}$$

cf. equation (61). Equation (81) serves as alternative approach to the ionization yield. The normalization $P_{bound} + P_{ion} = 1$ and $P_g + P_u = 1$ as well as good agreement of P_{ion} and $Y_{total,as}$, equations (81), (63), (64) and (69), as well as for the results for P_g and P_u according to equations (61) and (84) provide additional numerical tests of the consistency of the present TDEHF-SAE method. The advantage of expression (81) is that it allows the decomposition of the total ionization yield in terms of gerade and ungerade components of the ionized wavefunction.

The success of the present TDEHF-SAE approach relies not only on the validity of the conditions (i)–(vi) and (vii'), but also on adequate numerical grid representations of the wavefunction $\Psi(t)$, equation (18), in particular for the initial state $\Psi(t = 0)$, equation (1). In practice, the grid representations of the initial active orbital $\varphi(t = 0)$ is obtained by imaginary time propagation of the equations of motion for $\varphi(t)$, starting from the quantum chemical representation of the orbital $1\sigma_u$, similar to the technique of Ref. [28]. The inactive orbital $1\sigma_g$ remains frozen with its grid presenations adopted from the quantum chemical results. As a test of the validity of these grid representation of $1\sigma_g$ and $1\sigma_u$, we have calculated the initial energies $E(t = 0)$ when starting from the initial states $\varphi(0) = \frac{1}{2}1\sigma_g$ or $\varphi(0) = \frac{1}{\sqrt{2}}1\sigma_u$, cf. equations (20), (19), (40), (48). The results $E(t = 0) = -1.09868\,E_h$ and $-0.75092\,E_h$ agree well with the quantum chemical CASSCF(2,7) results for the ground and excited state energies at $R_{eB} = 2.2998\,a_0$, $E_{H_2(X^1\Sigma_g^+)} = -1.10803\,E_h$ and $E_{H_2(B^1\Sigma_u^+)} = -0.74785\,E_h$, respectively. For applications focussing on transitions to excited electronic states, the validity of the grid should also be tested for their energy levels. We aim, however, at TDEHF-SAE simulations of ionization by laser pulses, relying on all the other successful numerical tests as summarized above.

3 Results and Discussions

The applications of the TDEHF-SAE extension of Koopmans' theorem, section 2, will be presented in two steps: first, we consider an example, i.e. ionization of $H_2(B^1\Sigma_u^+) \rightarrow H_2^+(X^2\Sigma_g^+) + e^-$ by the five-cycle laser pulse (4) with photon energy $\hbar\omega = 8\,\mathrm{eV}$ and field strength $E_0 = 0.02\,E_h/ea_0 = 102.8\,\mathrm{MVcm^{-1}}$, corresponding to maximum intensity $I_{max} = 2.81 \cdot 10^{13}\,\mathrm{Wcm^{-2}}$. The laser pulse is shown in the top panel of figure 2. Subsequently, we present a systematic comparison of analogous results for weaker field strengths.

The total spectrum $\alpha(\omega)$ and its symmetry-adapted components $\alpha_g(\omega)$ and $\alpha_u(\omega)$ are shown in figure 1b, cf. equations (75), (76). Obviously, the spectrum is dominated by a huge, rather narrow peak for the ungerade initial state $B^1\Sigma_u^+$. The second important peak appears in the gerade spectrum $\alpha_g(\omega)$, close to the spectrum of the laser pulse $E(\omega)$, cf. equation (8) (i.e. with nearly the same broad width, $\Gamma = 2.31\,\mathrm{eV}$), but with much smaller ($< 1/1000$) height than the dominant peak close to $E_{H_2(B^1\Sigma_u^+)}$. Even much smaller spectral peaks, which are not visible on the grafical scale of figure 1b, appear in the ungerade and gerade spectra in the energetic domains for two and three photon transitions, respectively. This overall pattern of the symmetry resolved spectra shows that indeed, the laser pulse causes dominant single photon transitions from the ungerade initial state $B^1\Sigma_u^+$

to the gerade states embedded in the ionization continuum, in accord with conditions (iv)–(vi) for Koopmans' theorem. Quantitative confirmation is provided by the values for the corresponding probabilities, i.e. $P_{bound,u} = 0.93003$, $P_{ion,g} = 0.06612$, $P_{ion,u} = 0.00018$, $P_{bound,g} = 0.00012$. Most of $P_{ion,g}$ consists of the area under the peak for single photon ionization (= 0.06607), the rest (= 0.00005) may be attributed to three photon transitions. Likewise, $P_{ion,u}$ and $P_{bound,g}$ account for mainly two or three photon transitions, respectively. About one quarter (= 0.00003) of $P_{bound,g}$ is localized in the tiny peak close to $E_{H_2(E^1\Sigma_g^+)}$, cf. figure 1b. We note in passing that, gratifyingly, the $E^1\Sigma_g^+$ state has dominant electronic configuration $(1\sigma_g)(2\sigma_g)$, i.e. it may be well described within the present TDEHF-SAE approach. As a net result, the total ionization probability is

$$P_{ion} = P_{ion,g} + P_{ion,u} = 0.06630 \approx P_{ion,g}, \tag{85}$$

i.e. most of the ionized states have gerade symmetry.

Figure 2 shows important details of the wavepacket dynamics which is driven by the laser pulse (panel 2a, cf. figure 1b), as expressed by the time evolutions of various properties (panels 2b-e). These discover two important effects labelled A, B which occur during the laser pulse, $0 \le t \le t_p$: It causes (A) transient cycling between a small part of the ungerade initial state and gerade states embedded in the ionization continuum, with the same frequency as the laser pulse, but with a phase shift of approximately $\pi/2$. (B) Simultaneously, it induces persistent transitions from the initial state to the continuum states. Both effects may be interpreted in terms of the laser driven wavepacket dynamics, i.e. (A) the laser pulse shakes part of the wavepacket $\varphi(t)$, starting from the initial orbital $1\sigma_u$ which is occupied by the SAE, with rather small amplitudes and putting most of it back into $1\sigma_u$, at the end of the pulse. Simultaneously, (B) small fractions of the wavepacket are shaked away towards ionization, represented by gerade states. These effects are visible in various phenomena which are documented in figure 2. In particular, transitions from the initial state $B^1\Sigma_u^+$ to gerade states in the ionization continuum (B) (compare figure 1b) are obvious in the overall rather smooth increases of the population of the gerade states $P_g(t)$, and of the mean energy $\langle E(t)\rangle$, as well as in the overall decay of the modulus of the autocorrelation function $|C(t)|$, see panels 2d, 2e and 2c, respectively. These transitions (B) are superimposed by the oscillations due to phenomenon (A), with envelopes similar to that of the laser pulse, compare panels 2c-2e with 2a. In addition, the transient oscillations of the wave packet (A) are also visible in the mean values of the z-component of the dipole $M_z(t)$, equation (49). Note that at the end of the laser pulse, $M_z(t) \approx 0$ is almost back to its initial zero value (equation (52), in accord with the small transition probability to mainly gerade ionization states, except for a small deviation which will be discussed below, see equation (86) etc.

After the laser pulse, we observe three additional effects C, D, E, see the domains $t > t_p$ in panels 2b-2e: The first of these (C) is trivial within the present model which neglects nuclear motions and spontaneous emission, but nevertheless it is worth noticing, i.e. after the laser pulse, there are no additional transitions between electronic states. As a consequence, the modulus of the autocorrelation function $C(t)$ as well as the mean value of the

total energy $\langle E(t)\rangle$ remain constant, c.f. panels 2c and 2d, respectively. (D) The electronic states which have been excited to the ionization continuum (effect (B)) move towards the asymptotic domains, i.e. they run out of the grid. As a consequence, the probability $P_{gr}(t)$ of observing the wave function on the grid decays (panel 2c). The fact that the ionized states have almost exclusively gerade symmetry implies that the decay of $P_{gr}(t)$ is almost exclusively due to the corresponding decay of its gerade component, $P_{g,gr}(t)$, c.f. panel 2d. Panel 2d also shows that this decay is compensated by the corresponding increase of the ionization yield $Y_{total}(t)$. Note that the onset of $Y_{total}(t)$ occurs at $t_{gr} > t_p$, in accord with condition (68). The decomposition of $Y_{total}(t)$ into its components reveals two subtleties of effect (D): (D1) The fluxes of electrons towards ionization along the positive and negative z-axis are equal, within the grafical resolution of panel 2d. This is a consequence of the fact that the present photoionization (B) populates gerade ionization states almost exclusively. We note in passing that we have also carried out additional calculations for stronger field strength (cf. figure 4 below), demonstrating symmetry breaking due to enhanced two photon transitions to ungerade ionization states, but these are beyond the validity of conditions (iv)–(vi) of Koopmans' theorem and will, therefore, not be discussed with any further details. (D2) The ionization yields along the radial direction ρ is about equal to the sum of the ionization yield along $+z$ and $-z$. This is somewhat unexpected, because the laser drives the electronic wavepacket exclusively along $+z$ or $-z$, not along ρ. Apparently, the result (D2) indicates ultrafast dispersion of the ionized electronic wave packet towards all directions, including $+z$, $-z$ and ρ. This effect has been noted previously, e.g. it is inherent in the seminal paper on the simple SAE model of high harmonic generation by Corkum [45].

As anticipated in section 2, the results for the total ionization yield $Y_{total,as} = 0.06616$ and $1 - P_{gr}(t_{as}) = 0.06704$ ($t_{as} = 15.5\,\mathrm{fs}$) agree almost quantitively, and also with the value $P_{g,gr}(t_p) = 0.06633$, due to the fact that the ionized states have dominant gerade symmetry. Last but not least, it agrees well with the value $P_{ion} = 0.06630$ deduced from the spectra, cf. figure 1 and equation (85). The agreement of these four quantities demonstrates the intrinsic consistency of the present method. Numerically, the easiest way of determining the ionization yield is to calculate $P_{g,gr}$, because this costs the propagation of $\varphi(t)$ just during the laser pulse, $0 \le t \le t_p = 2.584\,\mathrm{fs}$. The calculations of $Y_{total,as}$ or $1 - P_{gr}(t_{as})$ are more demanding – they require propapagation of $\varphi(t)$ till $t_{as} = 15.5\,\mathrm{fs}$, plus the integration of accumulated fluxes for $Y_{total,as}$. The most demanding calculation has to be carried out for P_{ion}, i.e. propagation of $\varphi(t)$ till $T = 90\,\mathrm{fs}$, cf. figure 1b.

Finally, we observe effect (E), i.e. small amplitude oscillations of the mean z-component of the dipole $M_z(t)$, cf. equation (49) after the laser pulse, cf. panel 2b. It is rationalized in terms of a simple model of the time evolution of $\varphi(t)$ after the laser pulse, as follows: Let us decompose $\varphi(t > t_p)$ approximately into three contributions

$$\varphi(t) \;\approx\; c_B\, e^{-i\omega_B t}\, 1\sigma_u + c_E\, e^{-i\omega_E t}\, 2\sigma_g + \varphi_{ion,g}(t) \tag{86}$$

which describe the dominant partial wave that remains in the ungerade initial state $B^1\Sigma_u^+$, as well as the excited gerade bound state $E^1\Sigma_g^+$ (cf. the tiny peak in the excitation

spectrum, figure 1b) and the gerade ionization states, respectively. The bound states labelled $k = B = \mathrm{H}_2(B^1\Sigma_u^+)$ and $k = E = \mathrm{H}_2(E^1\Sigma_g^+)$ have corresponding amplitudes $|c_k|$, phases η_k and frequencies $\omega_k = E_k/\hbar$,

$$c_k e^{-i\omega_k t} = |c_k| e^{i(\eta_k - \omega_k t)}. \quad (87)$$

Inserting the ansatz (86) into the expression (49) for $M_z(t)$ yields six terms

$$\begin{aligned} M_z(t) \approx & -2e\left(|c_B|^2\langle 1\sigma_u|z|1\sigma_u\rangle + |c_E|^2\langle 2\sigma_g|z|2\sigma_g\rangle + \langle\varphi_{ion,g}(t)|z|\varphi_{ion,g}(t)\rangle\right) \\ & -4e|c_B||c_E|\langle 1\sigma_u|z|2\sigma_g\rangle\cos\left((\eta_B - \eta_E) + (\omega_E - \omega_B)t\right) \\ & -4e\,\mathrm{Re}\left(c_B\langle 1\sigma_u|z|\varphi_{ion,g}(t)\rangle e^{-i\omega_B t}\right) - 4e\,\mathrm{Re}\left(c_E\langle 2\sigma_g|z|\varphi_{ion,g}(t)\rangle e^{-i\omega_E t}\right). \quad (88) \end{aligned}$$

The first three and the last contributions in equation (88) vanish due to symmetry, and the fifth one is negligible because of the marginal overlap of the compact orbital $1\sigma_u$ and the product of z times the wide-spread partial wave $\varphi_{ion,g}(t)$. As a consequence, expression (88) reduces essentially to

$$M_z(t) \approx -4e|c_B||c_E|\langle 1\sigma_u|z|2\sigma_g\rangle\cos\left((\eta_B - \eta_E) + (\omega_E - \omega_B)t\right), \quad (89)$$

i.e. $M_z(t)$ should oscillate with period

$$\tau_{EB} = \frac{h}{E_{H_2(E^1\Sigma_g^+)} - E_{H_2(B^1\Sigma_u^+)}} \approx 4.19\,\mathrm{fs}, \quad (90)$$

in gratifying agreement with the period $\tau_M = 4.18\,\mathrm{fs}$ as deduced from panel 2b. Moreover, the average value of the amplitude $4e|c_B||c_E||\langle 1\sigma_u|z|2\sigma_g\rangle| \approx 0.02692\,ea_0$ of the oscillation of $M_z(t)$, together with the value $|c_B| = 0.96438$ deduced from the spectrum ($P_{bound,u} \approx |c_B|^2 = 0.93003$) and the value $|\langle 1\sigma_u|z|2\sigma_g\rangle| = 1.3485\,a_0$ allow to determine the amplitude $|c_E| = 0.00518$, in good agreement with the probability $P_E = |c_E|^2 = 0.00003$ of occupying state $E^1\Sigma_g^+$, as deduced from the spectrum (figure 1b). Finally, expression (89) for $M_z(t)$ allows to determine the relative phase $\eta_B - \eta_E = 0.2114$ of the initial and excited bound states.

Figure 3 shows the TDEHF-SAE for another laser which has the same parameters as the one shown in Figures 2a and 1b, except for a smaller laser field strength $E_0 = 0.005\,E_h/ea_0 = 25.7\,\mathrm{MVcm^{-1}}$ ($I_{max} = 1.75 \cdot 10^{12}\,\mathrm{Wcm^{-2}}$). The comparison shows that, on one hand, all effects (A)–(E) are qualitatively robust for both laser pulses; in particular, the oscillatory phenomena (A) and (E) agree well with each other, even for subtleties such as their phase shifts and envelopes. As a net result, there are hardly any significant deviations between these oscillatory patterns – as marginal exception we point to small differences in the time evolutions of $P_{g,gr}(t)$ close to the end of the laser pulses, cf. figures 2d and 3d. On the other hand, the reduction of the laser field amplitudes E_0 and corresponding values of the maximum intensity I_{max} by factors 4 and 16 induce corresponding decreases of the amplitudes of the oscillations, e.g. by a factor 4 for the mean dipole $M_z(t)$, and by a factor 16 for the total ionization yield Y_{total}, compare figures 2b, 3b and 2d, 3d, respectively.

Note that again, the results for $Y_{total,as} = 0.00429$, $1 - P_{gr}(t_{as}) = 0.00434$ ($t_{as} = 15.5\,\mathrm{fs}$) and $P_{g,gr}(t_p) = 0.00432$ agree well with each other, cf. figures 3c and 3d. This confirms the intrinsic consistency of the TDEHF-SAE method and techniques, even for rather weak laser pulses.

The examples shown in figures 1-3 suggest that the ionization yield increases linearly with the maximum intensity of the laser pulse,

$$Y_{total} = \mathrm{const} \cdot I_{max} \tag{91}$$

The relation (91) is confirmed by a systematic investigation for intensities I_{max} from ca $10^9\,\mathrm{Wcm}^{-2}$ to $10^{14}\,\mathrm{Wcm}^{-2}$. The results are documented in figure 4. They may be interpreted as confirmation of dominant single photon transitions, in accord with conditions (iv)–(vi) of Koopmans' theorem, analogous to the well known relation (91) which is implied by the golden rule for continuous wave lasers; similar results have been documented e.g. in Ref. [9]. Deviations from the linear relation (91) are observed for stronger intensities $I_{max} > 10^{14}\,\mathrm{Wcm}^{-2}$, indicating the onset of significant contributions of two or multiple photon transitions, or other strong field effects.

4 Summary and Outlook

This work provides the TDEHF-SAE extension of Koopmans' time-independent picture for ionization by a laser pulse, with explicit derivations for initial singlet states of two-electron systems. It is based on the ansatz (18) or, equivalently (13), for the laser driven orbital $\varphi(t)$ which is occupied by the SAE, while the other electron remains in the frozen orbital, in accord with Koopmans' picture. The equation of motion (34) for $\varphi(t)$ has been derived in section 2, based on the Dirac-Frenkel variation principle. In addition, the numerical techniques for solving the EOM (34) have been developed, based on the spatial and temporal grid representation of the wave function which has been developed in Ref. [22], combined with imaginary time propagation for the grid representation of the initial wavefunction, similar to Ref. [28], and the method of Manolopoulos for absorbing boundaries [44] (first application to electron dynamics!). The system, photoionization of z-aligned $H_2(B^1\Sigma_u^+)$ by an ultrashort z-linearly polarized laser pulse (different from the ubiquitious model of H_2 in the electronic ground state!) as well as the parameters of the laser pulse (photon energy $\hbar\omega = 8\,\mathrm{eV}$, pulse duration $t_p = 2.58477\,\mathrm{fs}$, "weak" intensities $I_{max} \leq 10^{14}\,\mathrm{Wcm}^{-2}$) have been choosen carefully, in order not to violate any of the conditions (i)–(vi) for the validity of Koopmans picture, see sections 1 and 2; in particular, they ensure the dominance of single photon ionization.

We have provided various analytical as well as computational tests of the self-consistency of the TDEHF-SAE approach. The analytical tests include the limit of zero field strength, i.e. vanishing laser pulse, as well as the asymptotic time limit when the ionized partial wave of $\varphi(t)$ has left towards large distances from the ion. In these limits, we recover the time-independent energy levels of the ground and first excited singlet states of the molecule, as well as Koopmans' result for the ionization potential related to the orbital

energy of the initial state, $IP_i = -\epsilon_i$ [1], respectively, in HF or EHF level of quantum chemistry, cf. equations (40)–(46). The numerical tests provide good agreement of the values for the ionization yields calculated by four different techniques: decays of the probability of the total and symmetry adapted gerade wave functions to remain on the grid domain which is centered around the initial molecule or final ion, integrated fluxes towards external domains, and integrated ionization spectra.

The results document linear increases of the ionization yields with maximum intensities $I_{max} < 10^{14}\,\mathrm{Wcm}^{-2}$, cf. equation (91) and figure 4, as expected for single photon transitions, by analogy with the golden rule expression for photoionization by continuous wave lasers. In addition, we discover a wealth of details of the time evolutions of various properties, e.g. the mean dipole $M_z(t)$ or mean energy $\langle E(t)\rangle$, which are documented in figures 2 and 3. An unexpected result is the robustness of transient oscillatory patterns which are superimposed on overall smooth persistent evolutions with respect to increasing laser intensities.

Even though the derivations and applications are within the validity of Koopmans' picture of single photon ionization in terms of a single active electron, applications of the TDEHF-SAE theory to extended domains may still be useful, e.g. serving as stimulating reference. For example, Corkum's model of high harmonic generation [45] describes ionization and recollisions of a dispersive single active electron quite successfully, at least as stimulating reference, even in the domain of strong laser intensities causing multiphoton transitions. This conjecture is also supported by the close analysis of small amplitude variations of $M_z(t)$ after the laser pulse (figure 2b, see the discussion of equations (86)–(90)): it yields a self-consistent interpetation in terms of the amplitude of an excited bound state which is excited presumably by a three-photon process, in accord with a tiny peak in the excitations spectrum (figure 1b), representing very small (0.00003) population. Other examples of theories which are applicable in domains even beyond the original assumptions are als encouraging, i.e. the Born-Oppenheimer separation is valid even beyond the domains of fast motions of light electrons versus slow motions of heavy nuclei, cf. [46].

The TDEHF-SAE approach avoids physical problems of the previous TDHF-SAE approach [3, 18, 20], equation (21), as discussed in section 2, at the expense of the more demanding equation of motion (34) which contains the necessary additional e.g. exchange terms beyond TDHF-SAE theory.

The present results will serve as a basis for extensions of the TDEHF-SAE approach to photoionization of molecules with two electrons in initial triplet states, as well as with many-electrons in various spin multiplicities. A necessary condition is the validity of Koopmans' traditional time-independent picture of single photon transitions, implying fair descriptions of the energy levels of the initial molecule and the final ion within HF or EHF levels of quantum chemistry, with frozen orbitals except for the one which is occupied by the electron to be ionized. The corresponding strong condition (i)–(iii) will possibly restrict applications to specific systems or classes of molecules. Promising candidates include e.g. photoionization of $\mathrm{AlCl}(X^1\Sigma^+)$ to $\mathrm{AlCl}^+(X^2\Sigma^+)$, compare with Refs. [47, 48]. The other conditions (iv)–(vi) may be verified by adequate choices of the laser parameters, as demonstrated for the present application to $\mathrm{H}_2(B^1\Sigma_u^+) \rightarrow \mathrm{H}_2^+(X^1\Sigma_g^+)$. It is encouraging

that the additional numerical efforts for these multi-electron systems will be restricted to propagations of again just a single time-dependent orbital occupied by the SAE, however with e.g. Coulomb and exchange couplings to all other electrons in many frozen orbitals. It is easy to predict that the scaling of these efforts for a single active electron with the number of coupled electrons in frozen orbitals should be advantageous, in comparison with the more demanding techniques for many active electrons, see e.g. Refs. [4–6, 10, 27–30].

Finally, the present TDEHF-SAE theory should also be extended to applications to longer pulse durations, calling for simultaneous propagations of the SAE and the nuclei, similar to exemplary extensions of theories from time-dependent electron dynamics to electron plus nuclear dynamics [10,14–16,22,49], as discussed in section 1. The challenge of this extension is also shared with complementary approaches e.g. by Cederbaum and coworkers [50] – and last but not least by Remacle and Levine [51], see the acknowledgement!

Acknowledgements

J. M. would like to dedicate this paper with gratitude to his academic teacher, Professor Raphy D. Levine (The Hebrew University Jerusalem), on the occasion of his 70th birthday. We thank PD Dr. A. Saenz (Humboldt University Berlin) for stimulating discussions of our and their TDEHF-SAE approaches during academic weekends in Kolberg and Münchehofe during june 2006 and 2007, respectively, in the frame of the Berlin network Sfb 450. I. B. would like to express his gratitude to Professor Leticia González (Universität Jena, previously at Freie Universität Berlin) for her efficient introduction into the art of time-independent quantum chemistry. Financial support by Deutsche Forschungsgemeinschaft (DFG, project Ma 515/23-1), Bundesagentur für Arbeit (to I. B.) and Fonds der chemischen Industrie is also gratefully acknowledged.

References

[1] T. Koopmans, Physica **1**, 104 (1933).

[2] L. S. Cederbaum, G. Hohlneicher, and W. von Niessen, Chem. Phys. Lett. **18**, 503 (1973).

[3] H. Yu and A. D. Bandrauk, J. Chem. Phys. **102**, 1257 (1995).

[4] K. Harumiya, I. Kawata, H. Kono, and Y. Fujimura, J. Chem. Phys. **113**, 8953 (2000).

[5] Y. Ohtsuki, M. Sugawara, H. Kono, and Y. Fujimura, Bull. Chem. Soc. Jpn. **74**, 1167 (2001).

[6] K. Harumiya, H. Kono, Y. Fujimura, I. Kawata, and A. D. Bandrauk, Phys. Rev. A **66**, 043403 (2002).

[7] M. Lein, T. Kreibich, E. K. U. Gross, and V. Engel, Phys. Rev. A **65**, 033403 (2002).

[8] M. Awasthi, Y. V. Vanne, and A. Saenz, J. Phys. B **38**, 3973 (2005).

[9] M. Awasthi and A. Saenz, J. Phys. B **39**, S389 (2006).

[10] H. Kono, Y. Sato, M. Kanno, K. Nakai, and T. Kato, Bull. Chem. Soc. Jpn. **79**, 196 (2006).

[11] N. A. Nguyen and A. D. Bandrauk, Phys. Rev. A **73**, 032708 (2006).

[12] C. B. Madsen and L. B. Madsen, Phys. Rev. A **74**, 023403 (2006).

[13] S. Baier, C. Ruiz, L. Plaja, and A. Becker, Phys. Rev. A **74**, 033405 (2006).

[14] A. Palacios, H. Bachau, and F. Martín, Phys. Rev. Lett. **96**, 143001 (2006).

[15] A. Palacios, H. Bachau, and F. Martín, Phys. Rev. A **75**, 013408 (2007).

[16] J. L. Sanz-Vicario, H. Bachau, and F. Martín, Phys. Rev. A **73**, 033410 (2006).

[17] F. Martín, J. Fernández, T. Havermeier, L. Foucar, T. Weber, K. Kreidi, M. Schöffler, L. Schmidt, T. Jahnke, O. Jagutzki, A. Czasch, E. P. Benis, T. Osipov, A. L. Landers, A. Belkacem, M. H. Prior, H. Schmidt-Böcking, C. L. Cocke, and R. Dörner, Science **315**, 629 (2007).

[18] L. A. A. Nikolopoulos, T. K. Kjeldsen, and L. B. Madsen, Phys. Rev. A **76**, 033402 (2007).

[19] K. C. Kulander, Phys. Rev. A **38**, 778 (1988).

[20] J. L. Krause, K. J. Schafer, and K. C. Kulander, Chem. Phys. Lett. **178**, 573 (1991).

[21] K. C. Kulander, K. J. Schafer, and J. L. Krause, in *Atoms in Intense Laser Fields*, edited by M. Gavrila (Academic Press, New York, 1992), p. 247.

[22] G. K. Paramonov, Chem. Phys. Lett. **411**, 350 (2005).

[23] K. C. Kulander, Phys. Rev. A **36**, 2726 (1987).

[24] M. S. Pinzola, P. Gavras, and T. W. Gorczyca, Phys. Rev. A **51**, 3999 (1995).

[25] T. Klamroth, Phys. Rev. B **68**, 245421 (2003).

[26] P. Krause, T. Klamroth, and P. Saalfrank, J. Chem. Phys. **123**, 074105 (2005).

[27] J. Zanghellini, M. Kitzler, C. Fabian, T. Brabec, and A. Scrinzi, Laser Phys. **13**, 1064 (2003).

[28] T. Kato and H. Kono, Chem. Phys. Lett. **392**, 533 (2004).

[29] M. Nest, T. Klamroth, and P. Saalfrank, J. Chem. Phys. **122**, 124102 (2005).

[30] J. Caillat, J. Zanghellini, M. Kitzler, O. Koch, W. Kreuzer, and A. Scrinzi, Phys. Rev. A **71**, 012712 (2005).

[31] M. Lezius, V. Blanchet, M. Y. Ivanov, and A. Stolow, J. Chem. Phys. **117**, 1575 (2002).

[32] W. Kołos and L. Wolniewicz, J. Chem. Phys. **43**, 2429 (1965).

[33] W. Kołos and L. Wolniewicz, J. Chem. Phys. **45**, 509 (1966).

[34] L. J. Schaad and W. V. Hicks, J. Chem. Phys. **53**, 851 (1970).

[35] National Institute of Standards and Technology, www.nist.gov.

[36] C. S. Sharma, J. Phys. B **2**, 1010 (1969).

[37] H. Stapelfeldt and T. Seideman, Rev. Mod. Phys. **75**, 543 (2003).

[38] S. Zou, Q. Ren, G. G. Balint-Kurti, and F. R. Manby, Phys. Rev. Lett. **96**, 243003 (2006).

[39] T. Ergler, A. Rudenko, B. Feuerstein, K. Zrost, C. D. Schröter, R. Moshammer, and J. Ullrich, Phys. Rev. Lett. **95**, 093001 (2005).

[40] A. S. Alnaser, T. Osipov, E. P. Benis, A. Wech, B. Shan, C. L. Cocke, X. M. Tong, and C. D. Lin, Phys. Rev. Lett. **91**, 163002 (2003).

[41] M. Gisselbrecht, M. Lavollée, A. Huetz, P. Bolognesi, L. Avaldi, D. P. Seccombe, and T. J. Reddish, Phys. Rev. Lett. **96**, 153002 (2006).

[42] I. V. Litvinyuk, F. Légaré, P. W. Dooley, D. M. Villeneuve, and P. B. Corkum, Phys. Rev. Lett. **94**, 033003 (2005).

[43] S. Chelkowski, A. D. Bandrauk, and A. Apolonski, Phys. Rev. A **70**, 013815 (2004).

[44] D. E. Manolopoulos, J. Chem. Phys. **117**, 9552 (2002).

[45] P. B. Corkum, Phys. Rev. Lett. **71**, 1994 (1993).

[46] S. Takahasi and K. Takatsuka, J. Chem. Phys. **124**, 144101 (2006).

[47] S. R. Langhoff, C. W. Bauschlicher, and P. R. Taylor, J. Chem. Phys. **88**, 5715 (1988).

[48] I. Barth, J. Manz, and L. Serrano-Andrés, Chem. Phys. (2007), in press.

[49] S. Chelkowski, A. D. Bandrauk, A. Staudte, and P. B. Corkum, Phys. Rev. A **76**, 013405 (2007).

[50] A. I. Kuleff, J. Breitbach, and L. S. Cederbaum, J. Chem. Phys. **123**, 044111 (2005).

[51] F. Remacle and R. D. Levine, Z. Phys. Chem. **221**, 647 (2007).

Figure Legends

Figure 1. Time-Dependent Extended Hartree-Fock Single Active Electron (TDEHF-SAE) extension of Koopmans' picture applied to ionization of (z-)aligned $H_2(B^1\Sigma_u^+)$ by a z-polarized five-cycle laser pulse (equation (4)) with parameters $E_0 = 0.02\,E_h/ea_0 = 102.8$ MVcm^{-1} ($I_{max} = 2.81 \cdot 10^{13}\,$Wcm^{-2}), $\hbar\omega = 8\,$eV, $t_p = 2.584\,$fs. Panel a): Potential energy curves versus bond distance R of H_2 in the electronic excited states $B^1\Sigma_u^+$ and $E^1\Sigma_g^+$, and for H_2^+ in the electronic ground state $X^2\Sigma_g^+$. The energy levels $E_{H_2(B^1\Sigma_u^+)}$, $E_{H_2(E^1\Sigma_g^+)}$, $E_{ion} = E_{H_2^+(X^2\Sigma_g^+)}$ at $R_{eB} = 2.2998\,a_0$ are shown by dashed horizontal lines. The dominant Franck-Condon type single photon transition from $H_2(B^1\Sigma_u^+)$ to $H_2^+(X^2\Sigma_g^+)$ is illustrated by the vertical arrow. Panel b): Laser spectrum (dotted line, equation (8), arbitrary units), and excitation spectrum $\alpha(\omega) = \alpha_g(\omega) + \alpha_u(\omega)$ (continuous line, equations (75), (76)). For energies below and above E_{ion}, the total spectrum is dominated by the ungerade and gerade symmetry components, respectively. The gerade spectrum $\alpha_g(\omega)$ (dashed line) is shown with scaling factor 1000, revealing a tiny peak close to $E_{H_2(E^1\Sigma_g^+)}$.

Figure 2. TDEHF-SAE simulation of the photoionization $H_2(B^1\Sigma_u^+) \rightarrow H_2^+(X^2\Sigma_g^+) + e^-$ by the z-polarized laser pulse as specified in figure 1. Panel a): Laser pulse (equation (4), continuous line) and envelope (dashed line). Panel b): Induced mean z-component of the dipole $M_z(t)$ (equation (49)). Panel c): Modulus of the autocorrelation function $C(t)$, (equqtion (50), continuous line) and the probability $P_{gr}(t) = \langle\Psi(t)|\Psi(t)\rangle_{gr} = P_{g,gr}(t) + P_{u,gr}(t)$ of observing the wavepacket $\Psi(t)$ on the grid (equation (64), dashed line). Panel d): Gerade symmetry component $P_{g,gr}(t)$ of $P_{gr}(t)$, and total ionization yield $Y_{total}(t) = Y_{z(-)}(t) + Y_{z(+)}(t) + Y_\rho(t)$ (equation (63)), evaluated as integrated fluxes of the wavefunction $\Psi(t)$ along the negative ($Y_{z(-)}(t)$) and positive ($Y_{z(+)}(t)$) z-axis (dashed line, indistinguishable within grafical resolution) or along ρ-axis ($Y_\rho(t)$) (dotted line) out of the grid into the gobbler domains. Panel e): Mean energy $\langle E(t)\rangle$, equation (48). The vertical lines indicate the total pulse duration t_p and the time $t_{gr} > t_p$ when the laser driven wavepacket $\Psi(t)$ leaves the grid, as indicated by the onset of the increases of the total ionization yield.

Figure 3. Same as figure 2, but for weaker field strength $E_0 = 0.005\,E_h/ea_0 = 25.7\,$MVcm^{-1} ($I_{max} = 1.75 \cdot 10^{12}\,$Wcm^{-2}).

Figure 4. Total ionization yield $Y_{total,as}$ (equations (63), (69), $t_{as} = 15.5\,$fs) versus intensity I_{max} (equation (5), logarithmic scales), for the system $H_2(B^1\Sigma_u^+) \rightarrow H_2^+(X^2\Sigma_g^+) + e^-$. Details of the laser driven wavepacket dynamics for the examples $I_{max} = 2.81 \cdot 10^{13}\,$Wcm^{-2} and $1.75 \cdot 10^{12}\,$Wcm^{-2} are shown in figures 1, 2 and 3, respectively. The TDEHF-SAE extension of Koopmans' picture is valid in the linear domain, $I_{max} < 10^{14}\,$Wcm^{-2}.

Figures

Figure 1

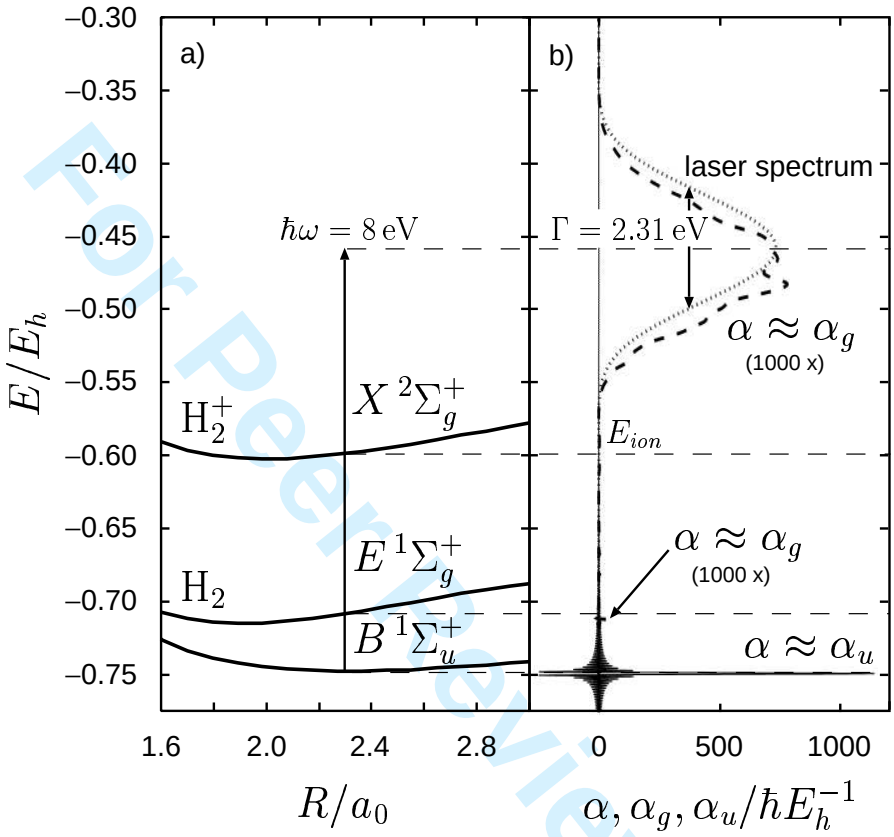

Figure 2

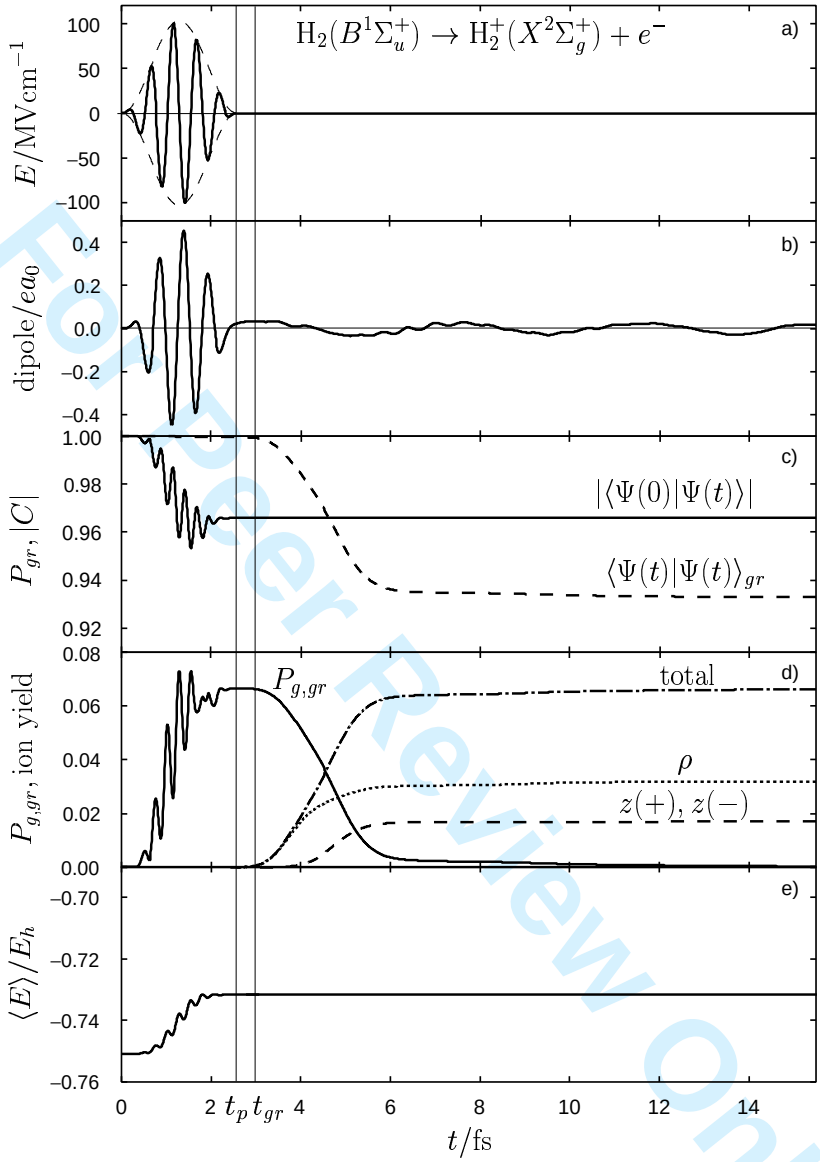

Figure 3

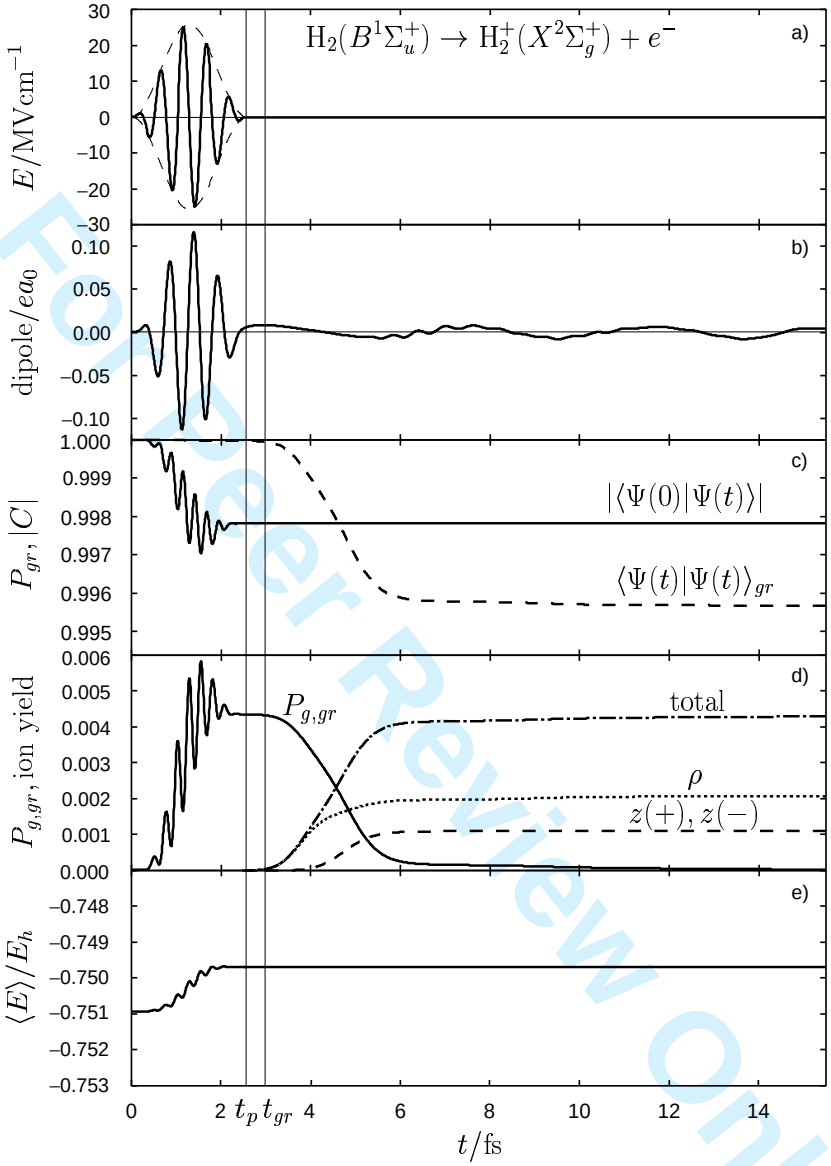

Figure 4